ALPHA DETECTION USING ZINC OXIDE NANORODS DEVELOPED THROUGH LOW TEMPERATURE HYDROTHERMAL GROWTH

A Master's Thesis
Presented to
The Academic Faculty

By

Stephen N. Hardwick

In Partial Fulfillment
of the Requirements for the Degree
Master of Science in Nuclear Engineering in the
Woodruff School of Mechanical Engineering

Georgia Institute of Technology

May 2017

ALPHA DETECTION USING ZINC OXIDE NANORODS DEVELOPED THROUGH LOW TEMPERATURE HYDROTHERMAL GROWTH

Approved by:

Dr. Hertel, Advisor
Woodruff School of Mechanical Engineering
Georgia Institute of Technology

Dr. Erikson
Woodruff School of Mechanical Engineering
Georgia Institute of Technology

Dr. Summers
School of Material Sciences and Engineering
Georgia Institute of Technology

Dr. Klein
School of Electrical Computer Engineering
Georgia Institute of Technology

Date Approved: April 13, 2017

If everyone tried to improve themselves and their environment one percent a day, how great would this world be?

Stephen N. Hardwick

To my wife, Laurin, and children, Smith and Sage. Your love and faith in me has driven me further then I could ever think possible.

ACKNOWLEDGEMENTS

I wish to thank my advisor, Dr. Nolan Hertel, for his support, guidance, and direction throughout the project and willingness to talk through any issues even during random flybys to his office. I would also like to thank my committee members, Dr. Christopher Summers, Dr. Benjamin Klein, and Dr. Anna Erickson, for their guidance and help as I worked through issues that came up during the project. The knowledge all of you bestowed upon me is much appreciated.

I would also like to thanks NNSA, NA-22, and the Consortia for Nonproliferation Enabling Capabilities for their funding of the project research and giving me opportunities for further education through conferences and providing a platform to present my findings.

To my fellow students and faculty as I quickly found without the support and help none of this would have been possible. When I came to Georgia Tech, I knew very little about nuclear engineering other then what I read in Lamarsh before I came, and with all the help from my officemates in 3-78, Drew, Omar, and numerous others, I was able to learn and understand many aspects of nuclear engineering. Thank you to Dr Shannon Yee for allowing me to use his research laboratory and equipment in the North Avenue Research Area.

Lastly, I would like to thank God and my family because without them I surely would have failed. Without their love and support, I would never have succeeded or become the person I am today.

TABLE OF CONTENTS

LIST OF TABLES

LIST OF FIGURES

SUMMARY

Zinc Oxide (ZnO) nanorods were grown using a low temperature hydrothermal process on a fused silica substrate. These nanrods were characterized using a scanning electron microscope (SEM), photo-luminescence (PL) spectra obtained using a Kimmon He-Cd laser, and radition spectra for Americium-241 (^{241}Am) obtained. The analysis of these results provides a broad baseline for future work to be conducted. This reasearch sought to make a detector capable of detecting alpha particles in order to be further adapted to detect neutrons in the future. The process taken in order to obtain these results started with the selection of a substrate and through the analysis of surface energy, transmission percentage for the near band edge emission of ZnO, and the cost. From this analysis fused silica was chosen. The next step was to successfully seed the substrate with a seed layer that covered the entire face of the substrate which was accomplished through using a spin coating technique. Growth of the nanorods was then conducted with dopants being indium and gallium with varying concentrations. Analysis of the nanorods was conducted using SEM imaging, PL spectra, and radiation detection. The results show a distinct effect of dopant and dopant concentration on the the detection spectra of ^{241}Am with results obtained by ZnO:In 1.0% showing most intense detection peak compared to gallium and undoped. Analysis of PL spectra and the effects of the dopants is still under much debate in the scientific community as the reason behind the green-yellow broad emission. Results can be improved by using polyetheyleneimine (PEI) and sodium citrate combination in order to lengthen the nanorods while also keeping lateral width which would benefit radiation detection ability allowing for full energy transfer of α-particles.

CHAPTER 1
INTRODUCTION

Ever since the discovery of radiation in 1895 when Wilhelm Conrad Roentgen noticed a florescence coming from an enclosed opaque tube due to electrical charge passed between two plates used for studying cathode rays, there has been an ever growing need and drive in nuclear sciences to both understand and detect radiation.[1] This drive led to further advancements in the area of radiation from understanding the particles individually to atoms to molecules as well as how to effectively and efficiently detect them. Many of the detection methods and detectors in use today are ones developed in the early to mid twentieth century which illustrates the difficulty in increasing efficiency of detecting ionizing radiation especially neutrons.

Detection of ionizing radiation has many applications from national security to the medical field. Within these applications lay many different methods and material for detection each of which is under constant research for better and more efficient means of detection. National security purposes seek to identify special nuclear material through both passive and active interrogation techniques at centers of mass transportation and ports that accept thousands of cargo containers and packages everyday. A commercial application of interest is well logging, which uses different sources of radiation to interrogate the ground as drilling is conducted in order to locate oil, gas, water, and mineral formations among other things.

Development of novel radiation detectors has always been and will always be an active area of research as the science of nuclear physics and engineering expands and the use of radioactive material widens. Refinement of new detection methods and detectors is key to many areas of industry and security. Each of these detectors has its pros and cons which always leads to the need for more efficient and better energy resolution detectors. Through

these demands for advancement, new technology for detection will be bred alongside new advancements in the field whether it is in energy, industrial use of radioactive isotopes or national security endeavors.

Zinc oxide (ZnO) is one of many new detectors in scintillation research being developed, and there has been limited use in research as an alpha detector in DT neutron generators to detect alpha particles.[2, 3] Promising characteristics of zinc oxide have a wide range of application not only in radiation detection as will be discussed in Section 2.3.3: Application in Fields of Science. The study of ZnO is not a new venture and has been studied and experimented with in its different forms since the early to mid twentieth century. Early mentions of ZnO as a inorganic crystal scintillation detector date back to as early as the 1960s, but its furtherment has not occurred until recently, particularly due to advances made due to its usefulness as a semiconductor and better technology and equipment to fabricate it. Zinc oxide has many uses and is found in many forms from powders to nanoparticles to nanorods used in various manners from sunscreen to solar panels. Since new methods of growth and fabrication of ZnO have increased and been refined using present day technology, there has been a rapid expansion and revival in ZnO and its characteristics mostly but not limited as its use as a semiconductor.[4] Some of those characteristics that are benefitial to all areas is its radiation hardness, thermal conductivity, and electron mobility.[4, 5, 6]

1.1 Objective

The objective of this thesis is to develop a zinc oxide alpha detector using low cost hydrothermal method and to set a solid baseline for future research to build off of. The detection medium will consist of uniform uni-axial grown ZnO nanorods across the face of a 50.8 mm fused silica substrate. This broad scope of research includes substrate anaylsis, seeding process experimentation, characterization of seed layers and grown crystals with a scanning electron microscope, photo-luminescence spectra, and radiation detection

of Americium-241(^{241}Am) α-particles. Through the analysis and experiments from this work, future work can be conducted in order to develop ZnO nanorod detection system into a neutron detector. Due to its high radiation hardness characteristics which will be discussed in the next chapter, ZnO has a wide range of uses in terms of radiation detection.

Characterization of the seed layer and the grown nanostructure using a scanning electron microscope (SEM) objectives include verification of a seed layer that covers the face of the substrate that the nanorods will be grown on. The objective of the characterization of the nanorods is to make sure that there is dense uniform growth across the entire face of the detection area along the c-axis (vertical). Other objectives of characterization using a SEM include taking length measurements and width measurements. Using these characteristics, the effect of dopants on the crystal structure are analyzed.

The objective of photo-luminescence spectra analysis is to be able to verify the near band edge emission peak of ZnO as seen in literature and to analyze the effect of dopant and dopant concentration on the spectra. Through this and analysis and information in literature, a better understanding of the effects can be made. The intensity of light emission is also telling of the number of photons that will likely be emitted when an energetic charged particle passes through it.

With respect to the detector, the objective is to detect alpha particles and the effect of different dopants on the spectra. Being able to detect alpha particles with a strong response is needed in order for further research to be conducted into its ability to detect neutrons through interaction with a neutron absorber such as lithium-6 (^{6}Li) or boron-10 (^{10}B) which emit an alpha particle upon absorption at a very high percentage.

CHAPTER 2
BACKGROUND INFORMATION

In order to understand the research conducted in this project, a basic understanding of interaction of charged particle radiation with matter is needed. The radiation physics behind how these particles interact with matter are important to have at least a basic understanding of and will be a topic of discussion in this chapter. Past the radiation physics of these interactions, the science behind how these physics apply directly to detecting the particles themselves and extracting information about the radiation is the next logical step.

Since radiation was discovered, there has been a never ending search for better material and methods of detecting them as these particles can both be helpful, such as treating cancer, and very devastating, such as the atomic bomb. With the state of the world today and actions of non-state actors seeking special nuclear material (SNM), the need for new and innovative detection media will continue to be a viable area of research for the near and long term. There are different methods of detection of radiation from gas proportional counters to semi-conductors to scintillators. Scintillation detection is the primary topic of interest in this research project and is discussed in the following sections.

Zinc oxide (ZnO) nanorods have been widely researched for the purposes of its n-type semiconducting properties and their potential use in solar power collection in favor of the very toxic and environmentally unsafe manner they are presently constructed. An overview of the effects of zinc oxide nanoparticles and nanorods on science, research and industry, will be briefly discussed in this chapter as well as an overview of the growth mechanism and crystal structure for the formation of zinc oxide nanorods.

2.1 Charged Particle Interaction with Matter

Charged particles, for example α-particles, rarely interact with a nuclei and instead interact mainly with atoms via coulomb forces with electrons. As such, because the large mass difference between a heavy charge particle and an electron, the path or trajectory of a charged particle in matter is not easily altered unless interaction with nuclei in the form of elastic collisions occur. An alpha particle interaction with electrons through coulomb forces causes energy to be transfered to the electron exciting it. This results in the molecule either being ionized (loss of electron) or reaching an excited state (electron promotion to higher shell).

$$(\frac{dE}{dx})_c = \frac{4\pi z^2 k_c^2 e^4 NZ}{mc^2\beta^2}[ln(\frac{2mc^2\beta^2}{I}) - ln(1-\beta^2) - \beta^2] \tag{2.1}$$

$$\begin{aligned} I &= 19.0\ eV,\ Z = 1 \\ I &= 11.2 + 11.7Z\ eV,\ 2 \leq Z \leq 13 \\ I &= 52.8 + 8.81Z\ eV,\ Z > 13 \end{aligned} \tag{2.2}$$

Of key importance to charged particle interactionand range in matter is the collisional stopping power equation, which is shown in Equation 2.1.[7] In this equation, z is equal to the charge of the charged particle; k_c is equal to $\frac{1}{4\pi\epsilon_0}$ and ϵ_0 is the dielectric constant in vacuum; e is equal to the charge of electron; NZ is equal to the number of electrons per unit volume; $mc^2\beta^2$ is equal to the relativistic mass of electron; and I is constant derived from empirical formula that is dependent on the Z of the material/element that the charged particle is interacting with as shown in Equation 2.2.[7] When the resulting stopping power is divided by the density (ρ), the mass stopping power of the detection medium is obtained.

The range of charge particles is generally much more defined then that of uncharged particles, such as neutrons and gamma rays, because charged particles are constantly un-

dergoing inelastic collisions in a continuous slowing down effect. Heavy charged particles such as an α-particle have an even more defined range due to losing their energy in smaller quantities per collision then a lighter charged particle, for example an electron or proton.

A well researched and important characteristic to the range of heavy charged particles is the Bragg curve. The principle to be taken from the Bragg curve is that a heavy charge particle loses most of its energy near the end of its range in the matter and will form a peak and quickly go to zero. This is important in the deposit of energy into the detector. If the detector thickness is small compared to the range of the charged particle in that particular matter then minimal energy will be deposited resulting in a weak response in terms of particle detection and electron excitation. If the detector thickness is near or slightly larger then projected range, the response of the detector will be much stronger than that of a detector whose thickness is prior to the bragg peak for the given material.

2.2 Scintillation Detection of Radiation

There are several methods and detectors for the detection of ionizing radiation. Of importance to this thesis is scintillation detection of ionizing radiation which is the process of exciting electrons from the valence band to the conduction band and emission of light photons upon return to the valence band. There is, however, more then just the luminescence route, for example quenching, that an electron can take in returning to the valence band. Following light emission, there are mechanisms that prevent the light collection and are unavoidable. Self-absorption, light trapping, and internal reflection are all examples of effects that will prevent light photons from reaching the photomultiplier tube (PMT). The minimization of these effects will allow more light generation and light reaching the PMT for conversion into a signal.

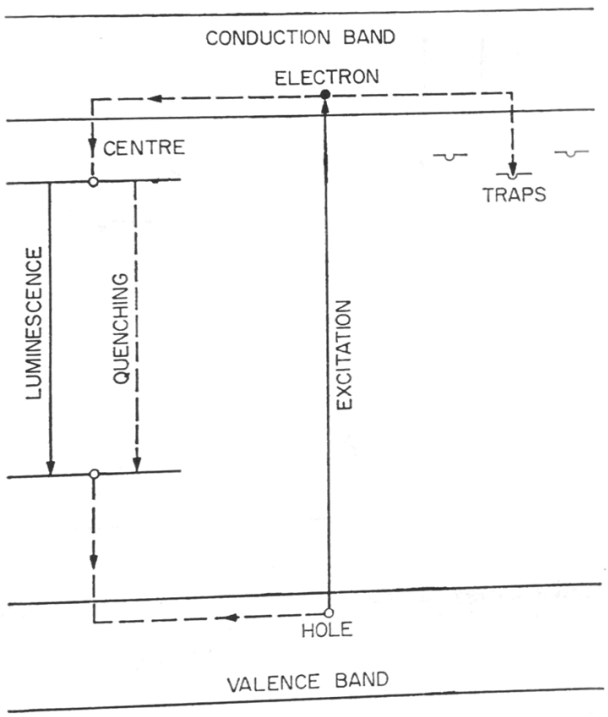

Figure 2.1: Energy bands in impurity activated crystal phosphor, showing excitation, luminescence, quenching and trapping processes[8]

2.2.1 Process/Mechanism of Scintillation

Figures 2.1 and 2.2 refer to the scintillation mechanism of inorganic crystals as a whole. The exception for zinc oxide is that due to its low band gap in comparison to other inorganic scintillation detectors activators are not needed in order to generate an acceptable number of scintillation photons. This is called having direct band gap response. Because of this, electrons do not have to travel to activator sites while in the conduction band to return to the

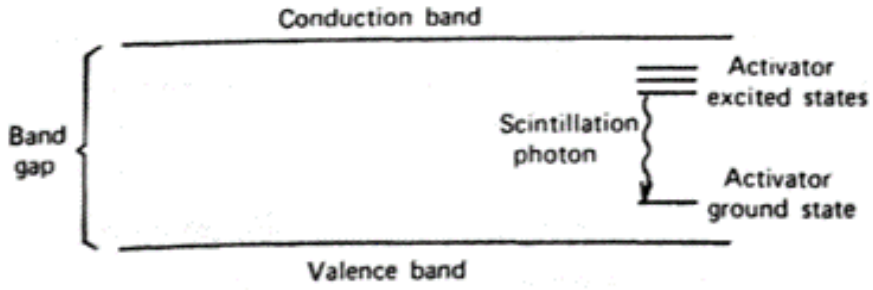

Figure 2.2: Energy band structure of activated crystal[9]

valence band. Once excited, the electrons only have to move to a hole in the valence band and cross the direct band gap. Because a hole is created when the electron is promoted to the conduction band, the distance to travel is minimal in most cases allowing for very fast response times, usually less than 10 ns. The valence band of the crystal represents the electrons that are bound tightly to the lattice structure and have little if any ability to move throughout the detector. Electrons in the conduction band are loosely bound to the lattice and can move freely within the crystal. The band in between the conduction band and the valence band is known as the forbidden band and electrons cannot be found there. In this band is generally where activators lie, slightly above valence band for its valence band and below the conduction band of the crystal. This allows for electrons to migrate to the activator sites which reduce the threshold that the electrons must cross to return to the valence band, but due to low percentage of activator sites, the response time is lengthened. For example, the decay time for sodium iodide (NaI) is 230 ns, and cesium iodide (CsI) is 680 ns.[9]

In order to create and electron-hole pair, on average it take three times the band gap energy.[9] Therefore, with the average band gap of ZnO, approximately 3.3 eV, it takes approximately 9.9 eV to create one electron-hole pair. The light energy and number of photons produced will correspond to electron-hole pairs which result in photon emission. Because ZnO is a direct band gap scintillator or pure crystal scintillator the energy released or liberated during recombination of the electron with the hole is roughly that of the energy required to promote the electron to the conduction band which will result in overlap of the absorption and transmission spectra.[9] This is talked about later in Section 2.2.2.

Photomultiplier tubes (PMTs) are often used with scintillatior detectors in order to convert light into a signal to be processed. As seen in Figure 2.3, the light enters the top of the PMT at the photocathode where it proceeds to dynode number one in the electron multiplier region. While in the photocathode region, the energy from the light is transfered to an electron that proceeds to the first dynode of the electron multiplication region. As it

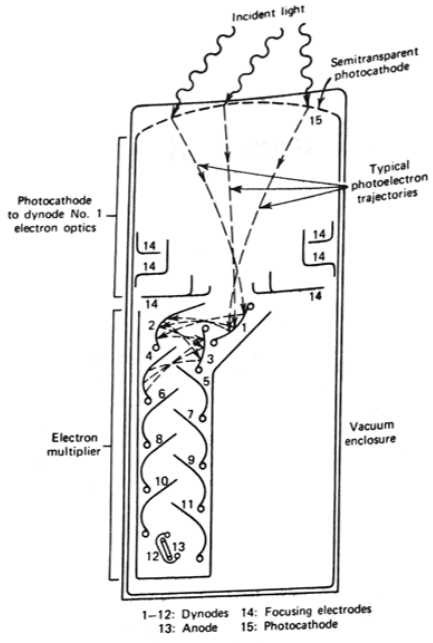

Figure 2.3: Basic Elements of a PM tube[9]

passes through the dynodes the electrons are multiplied until it reaches the bottom where the signal is sent to a preamplifier at the anode.

2.2.2 Quenching, Self Absorption and Light Trapping

Just as important as it is in understanding the mechanism by which light photons are created in scintillation, it is equally important to understand the mechanisms that both prevent emission and prevent light from reaching the PMT and registering an event. Understanding these effects and then being able to minimize their impact is important to all scintillation research. Quenching, whether internal to the lattice or molecules bonded to the lattice surface, causes electrons to return to the ground state or valence band without there being an emission. The two main ways that light is lost are through self absorption and light trapping. Self absorption occurs when light is created and then absorbed within the crystal, and light trapping occurs as a result of refractive index and will self reflect a fraction internally of the light with in the crystal structure trapping it.

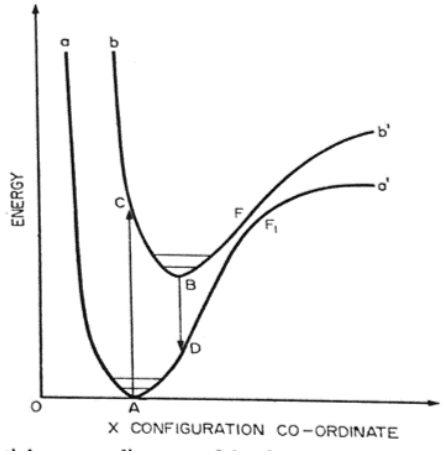

(a) Potential energy diagram of luminescence center or molecule. aAa', ground state. bBb', excited state. AC, absorption transition. BD, luminescence emission transition. FF_1, region of internal quenching.[8]

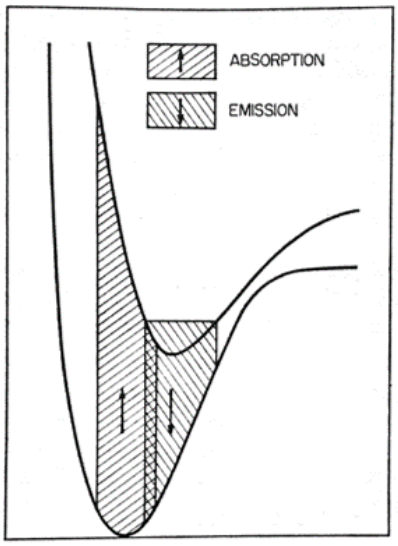

(b) Absorption and luminescence emission transmission showing origin of overlap[8]

Figure 2.4: Process of emission and areas that can result either in self absorption[8]

Quenching

The emission of a light photon as discussed in the previous section is only one way that an electron returns to the ground state or a state in which the energy and spin are satisfied. As can be seen in Figure 2.1, there are other pathways for an electron to return to the ground state besides the emission of a light photon in the process of crossing a direct bandgap, for example quenching.

Quenching is an alternate path that an electron can take to transfer its energy and return to the valence band, and it can occur either internally to the crystal (internal quenching) or through a molecule or atom in the vicinity of the excited electron. Important in this is electron transport and the ability of the electron movement in the conduction band to a center where it will deexcite to valence band. Internal quenching occurs within the lattice structure when an electron finds an alternate path to the valence band. As shown in Figure 2.4a, there is an area in the curve where the excited and ground state energy bands near intersection (F and F_1). If an electron is excited and makes its way to this spot then the energy difference is very small and will be absorbed thermally in the crystal and return to a lower vibrational state through vibrational relaxation. Another pathway to quenching would involve electron transport to a quencher molecule. If a molecule containing elemental oxygen was bonded and in close proximity to the electron excitation, then the electron would readily be accepted by oxygen and transfer energy thermally and through vibrational relaxation to the ground state. The effect of oxygen as a quencher is well researched and effect most areas of scintillation research.[10, 11, 12]

Self-Absorption

Even after scintillation light is produced via the deexcitation of electrons, there are mechanisms working against it such as self-absorption and light trapping, which will be discussed in the next section. One of the draw backs of pure crystal scintillators is the fact that there will be self-absorption of light emitted. The reason for this self-absorption is because the

energy required to excite and electron and create and electron-hole pair is roughly equal to that of the energy released during de-excitement which will cause the absorption and emission spectra to overlap causing self absorption.[9] In other words, it occurs when there is an overlap in the relative positions of the potential energy curve wells of the ground and excited states as shown in Figure 2.4b. In inorganic crystals this is quite common, and the way that it is combated is through the use of activator impurities which essentially shift the near band edge emission peak to the right past the absorption line so that it is not effected. This effect is less extensive in organic and plastic scintillators because there is less volume with respect to light emitting molecules.[8]

Light Trapping

Light trapping is when a light photon is internally reflected within the crystal and does not escape in order to be picked up by the PMT.[8]

$$\mu^2 = 2.81418 + \frac{0.87968\lambda^2}{\lambda^2 - 0.3042^2} - 0.00711\lambda^2 \tag{2.3}$$

$$\mu^2 - 1 = \frac{0.6961663\lambda^2}{\lambda^2 - 0.0684043^2} + \frac{0.4079426\lambda^2}{\lambda^2 - 0.1162414^2} + \frac{0.8974764\lambda^2}{\lambda^2 - 9.896161^2} \tag{2.4}$$

$$C = Sin^{-1}\frac{1}{\mu} \tag{2.5}$$

$$\frac{(\mu - 1)^2}{(\mu + 1)^2} = Fraction\ Internally\ Reflected \tag{2.6}$$

$$Fraction\ Entrapped = 3cos(C) - 2 \tag{2.7}$$

Using equations 2.3-2.7, as well as information obtained from [13], several important properties were calculated to better understand the fraction of light produced that will not be

detected because it will never reach the PMT. Equations 2.3 and 2.4 is used to calculate the refractive index for a particular wavelength (λ) for zinc oxide crystal and fused silica respectively.[14, 15, 16] Equation 2.5 calculates the critical angle for a given refractive index which can be used to calculate Equation 2.7 which is light that will be permenantly entrapped.[8] Equation 2.6 is the percentage of light that will be reflected internally and absorbed at the air interface.[8] This fraction is not known for the ZnO and fused silica interface. The fraction lost at the interface between fused silica and the PMT is minimized using silicon optical grease. These equations were used to calculate the fractions of light that will not make it to the PMT which needs to be taken into account and the values for these different properties are listed in Table 2.1.

Table 2.1: Zinc Oxide and Fused Silica Properties[8, 13, 16, 15, 17, 14, 18]

Property	Zinc Oxide (Bond)	Zinc Oxide (Querry)	Fused Silica
Refractive Index	2.294	1.6140	1.4725
Critical Angle(^{o})	25.8	38.3	42.8
Percent Internally Reflected(%)	15.4	5.52	3.65
Fraction Trapped	0.701	0.354	0.201

2.3 ZnO Methods Overview and Applications in Fields of Science

2.3.1 Methods of Synthesis, Structure, and Emission

There are several methods to grow the nanorods or other nanoparticles for development of a ZnO detector either as a single crystal or array of nanorods such as bulk melt[19], metal-organic chemical vapor deposition (MOCVD)[20], cathodic magnetron sputtering and reactive electron beam evaporation[21], spray pyrolysis[22], and electrodeposition[23]. The draw back from these methods are several fold in that the cost of production is very high due to equipment needed to produce the samples, the scale to which they can produce samples, and the quality and type of structures produced for their varying application varies

with each. Using a low temperature hydrothermal method, a large area detector can be grown on variety of substrates producing a dense array of nanorods with good crystalline structure along one axis and is a fraction of the cost of the other methods.

For a hydrothermal growth process in solution, there are also a variety of methods with respect to the reactants used, but most revolve around the use of either zinc nitrate hexahydrate or zince acetate dihydrate. The main variant in research is how the population of hydroxyl groups (OH^-) and zinc ions (Zn^{2+}) are produced. In this project, hexamethyleneamine (HTMA) and zinc nitrate hexahydrate were used. The formation of ZnO, GZO, and IZO using HMTA can be summarized by the following chemical equations [24]:

$$(CH_2)_6N_4 + 6H_2O \rightarrow 5COH_2 + 4NH_3 \tag{2.8}$$

$$NH_3 + H_2O \rightarrow NH_4^+ + OH^- \tag{2.9}$$

$$Zn(NO_3)_2 \cdot 6H_2O \rightarrow Zn^{2+} + 2NO_3^- + 6H_2O \tag{2.10}$$

$$Zn^{2+} + 2OH^- \rightarrow Zn(OH)_2 \rightarrow ZnO + H_2O \tag{2.11}$$

$$Ga(NO_3)_3 \cdot xH_2O \rightarrow Ga^{3+} + 3NO_3^- + xH_2O \tag{2.12}$$

$$4Ga^{3+} + 12OH^- \rightarrow 2Ga_2O_3 + 6H_2O \tag{2.13}$$

$$In(NO_3)_3 \cdot xH_2O \rightarrow In^{3+} + 3NO_3^- + xH_2O \tag{2.14}$$

$$4In^{3+} + 12OH^- \rightarrow 2In_2O_3 + 6H_2O \tag{2.15}$$

The molarity of the different additives from Equations 2.8-2.15 can be varied and changed to achieve the results that are needed for its desired use. Hydrothermal growth process usually entails suspending the substrate to be grown on upside down with the growth surface floating on top of the solution. Temperature of growth using various temperatures from 60-100^{o}C has been achieved and can be readily found in literature.[25, 26] Generally, the temperature if kept under 100^{o}C due to boiling temperature of the water molecules in

the solution.

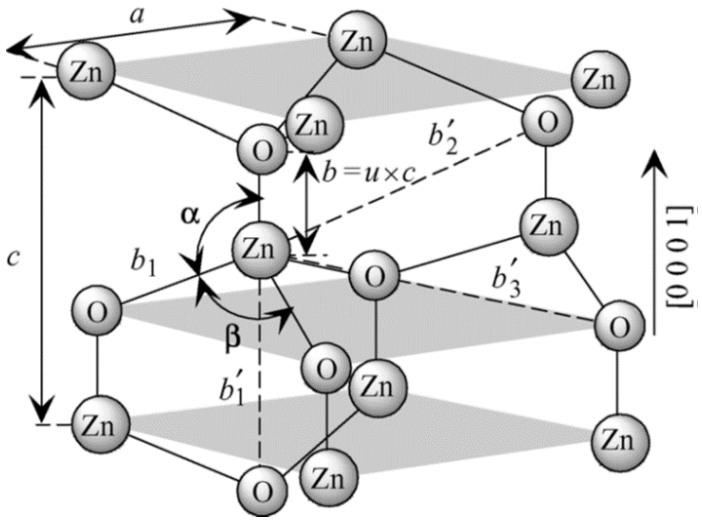

Figure 2.5: Schematic representation of a wurtzite ZnO structure[27]

The wurtzite structure of ZnO is well known and well researched. Research into ZnO typically involves altering the wurtzite structure in different ways such as increasing bond lengths and angles through the addition of dopants which replace Zn^{2+} ions within the lattice structure or migrate into interstitial spaces. The lattice constants of pure, perfect ZnO wurtzite crystalline structre are a = 0.3296 nm and c = 0.526065 nm which are present in the hexagonal structure with zinc and oxygen ions on alternate planes.[25] The location of the ions on different planes yielding a polar molecule can be seen in Figure 2.5.

The largest area of contention within the scientific community is the analysis of the photo-luminescence emission spectra and the cause of the different peaks. The broad green peak found in photo-luminescence spectra of ZnO has been proposed to be due to the zinc vacancies [4], which was contested and said to be caused by oxygen vacancies or zinc interstitials.[28, 29] Furthermore, there has been literature that claims that impurity defects within the lattice structure are the result of the green emission and yellow emission from the presence of hydroxyl groups and not interstitial oxygen or zinc vacancies.[30] The suppression of the broad green-yellow peak can be achieved or reduced through many methods whether it is dopants or annealing methods. This area of contention needs further

investigation so that ways to further suppress or enhance the broad peak can be properly addressed.

Indium and Gallium Dopant

A variable introduced into this research was the use of dopants in order to assess the changes in structure as well as performance with respect to photo-luminescence spectra and radiation detection. Dopants have been shown to alter performance characteristics such as a shift in the emission spectrum, supression of parts of the emission spectrum, and a change in band gap energy needed to create the light emission. The two dopants that were chosen for this research are indium(III) and gallium(III).

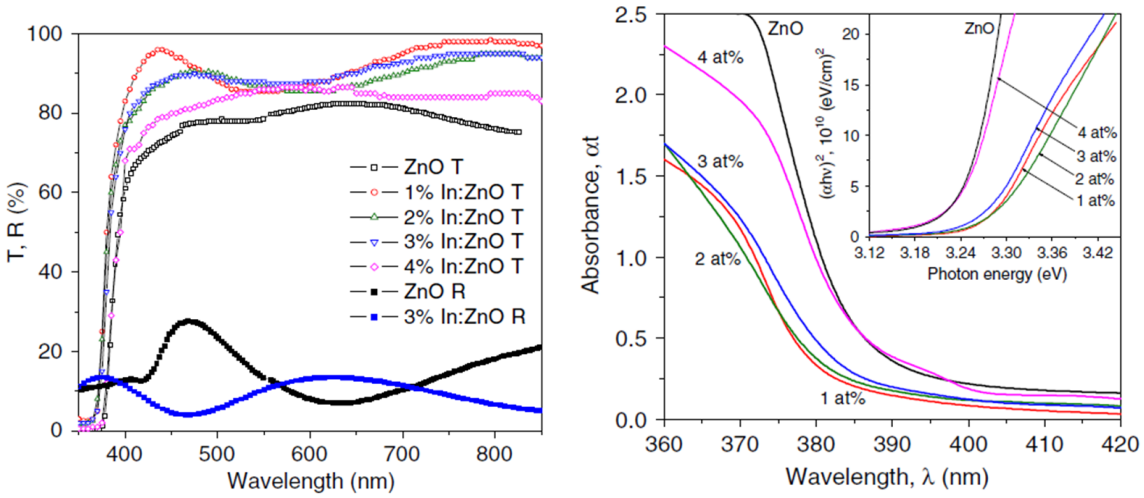

(a) Optical transmission and reflectance spectra of ZnO:In films

(b) Optical absorbance spectra of ZnO:In films. Inset shows plot of $(\alpha hv)^2$ versus photon energy

Figure 2.6: Reference information for choosing indium(III) as a dopant.[31]

Indium(III) in the form of indium(III) nitrate was chosen as a dopant for a few reasons, for example shifting of the transmission spectra and decrease in absorbance near the band edge light emission. A draw back of indium(III) is that the band gap does increase with the added impurity in the crystal, but the increase is only approximately 0.04 eV from 3.24 to 3.28 eV.[31] The reason that the band gap increases is explained in terms of Burstein-Moss band gap widening, which says that the increase in the Fermi level in the conduction band

due to the impurity leads to the band gap energy broadening. According to this effect, a higher concentration of impurity will result in a larger broadening of the gap.[31, 32] As can be seen in Figures 2.6a and 2.6b, there are significant changes in the transmission and absorption spectra generated when ZnO is doped with indium. In all cases, except for doping with high concentrations 4% and above, the transmission and absorption change to make the use of ZnO:In favorable. The shift of the transmission percentage to the left and absorption down prior to the 380 nm wavelength is ideal due to the near band edge light emission by ZnO. As with most dopants, there is some suppression of the emission peaks, but the shift will minimize the effect.

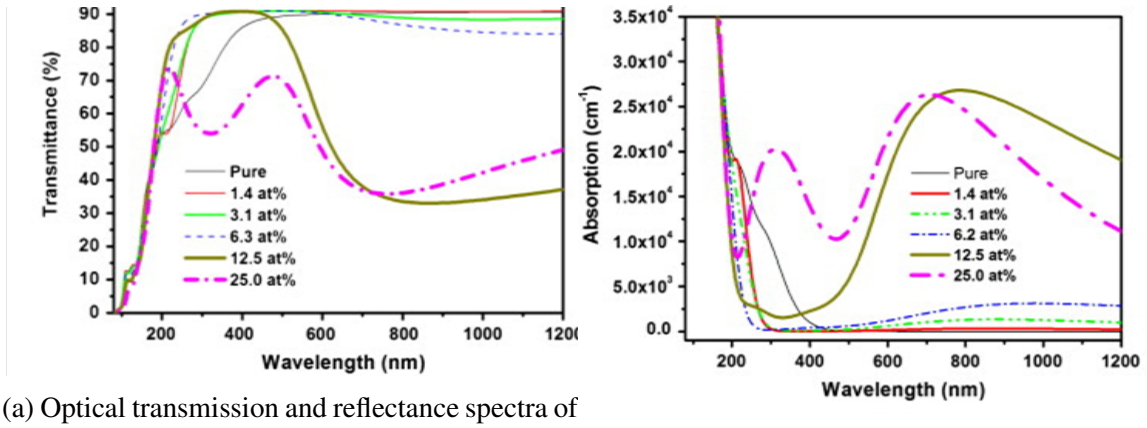

(a) Optical transmission and reflectance spectra of ZnO:Ga films

(b) Optical absorbance spectra of ZnO:Ga films.

Figure 2.7: Reference information for choosing gallium(III) as a dopant.[33]

Gallium has been used in several studies with varying degrees of success in attempt to enhance optical and electrical characteristics of ZnO nanorods, which both have a direct relationship to its ability to detect radiation. Similarly to other dopants, gallium shifts the transmission and absorption spectra and affects the intensity of both the ultraviolet and green impurity emission. While with other dopants the impurity generally shifts the transmission spectrum further left into ultraviolet, gallium has been shown to shift the spectrum to the right as shown in Figures 2.7a and 2.7b, which could cause some of the ultraviolet emission at 380 nm that is emitted upon de-excitation to be self-absorbed within the crystal without making to the photomultiplier tube to register an event.[24, 33] A partial

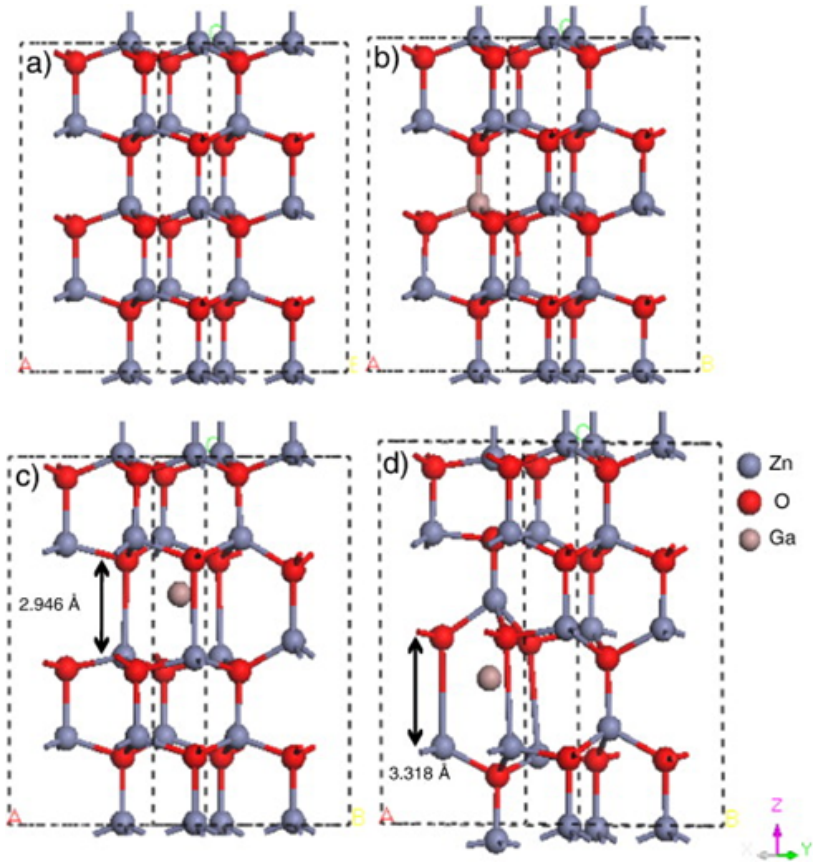

Figure 2.8: Models of ZnO:Ga a)pure; b)substitution doping; and interstitial site in c) octahedron and d)tetrahedron[34]

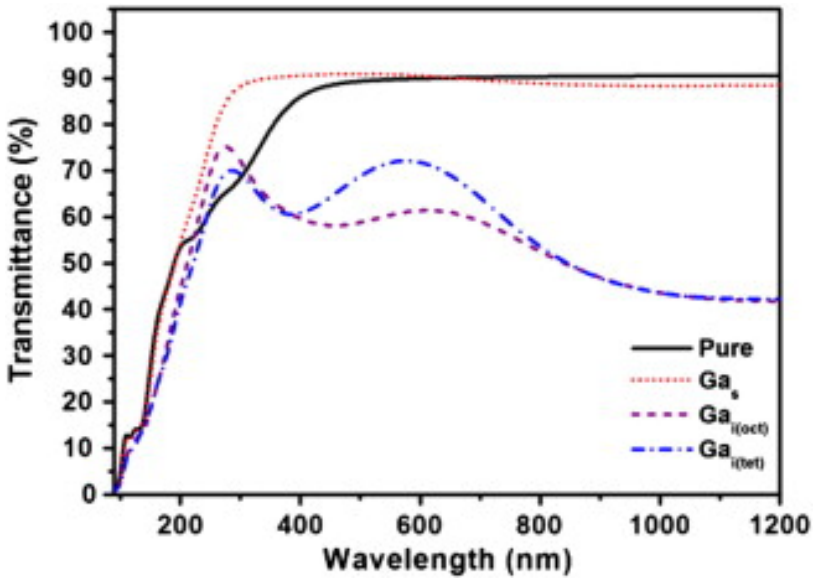

Figure 2.9: Transmission spectra of GZO using the ZnO:Ga models[34]

explanation can by surmised from [34] which used a theoretical approach using different locations for the gallium dopant as shown in Figure 2.8. The four cases shown in [34] are undoped, lattice substitution of Zn^{2+} with Ga^{3+}, and two interstitial location (tetrahedron and octahedron) which effect bond length and angles. As shown in Figure 2.9, the different models produce very different results with respect to the transmission spectrum. What can be surmised from this spectra is that the experimental spectrum achieved will most likely be a combination of the three dopant locationswith a shift in the spectra resulting in varying degress of emission suppression. Gallium has been used as a dopant in ZnO thin film [35] and bulk melt single crystals [19] for α-particle detection as a scintillator as well as the subject for investigation into optical qualities which is what drove the incorporation of gallium doping into the scope of this project.

Sodium Citrate Protocol

Sodium citrate as an additive to the ZnO growth process and effect on the ability to modify the growth habits of ZnO is known. The modification to the growth habits is the promotion of lateral growth in addition to the already preferred vertical growth to obtain wider nanorod structures.[36] This is accomplished due to the vertical growth being stunted because the presence of citrate anions in the aqueous solution results in the complexation of Zn^{2+} with citrate anions.[37, 38] Essentially, by adding sodium citrate, Zn^{2+} ions can be inhibited from attaching to the vertical component of the wurtzite structure allowing for larger lateral growth. With sufficient Zn^{2+} ions in comparison to citrate anions, there will still be significant growth along the c-axis, but the inclusion of the citrate will also allow for more lateral growth. Electron transport crystal to crystal is unknown, but assumed inefficient in comparison to migration within parent crystal; therefore, a wider nanorod should provide more luminescence centers for electrons to migrate to.

2.3.2 Applications in Fields of Science

Zinc Oxide in its many forms is the subject of research across various fields of science for its many different properties. Most of the application involve the semi-conductor characteristics but are generally limited to n-type semi-conducting applications as a viable and reliable method for p-type construction has yet to be achieved with any consistency although there are reports of breakthroughs. Due to its electron mobility, thermal conductivity, band gap characteristics, and exciton binding energy, ZnO can be made suitable for devices such as transistors, photodetectors, and light/laser diodes that operate in the UV/blue region.[4] Zinc oxide has also shown promise as a thin film scintillator for the detection of alpha radiation and been used in DT neutron generators used for detection of special nuclear materials.[39] Another area that ZnO has been applied is in the area of solar cell research. As research and development moves away from concentional photovolatic solar cells and towards excitonic solar cells, ZnO becomes a prime candidate due to its high electron mobility and wide surface area.[40]

Zinc oxide, due to its radiation hardness, has far reaching application not just on Earth but in space with little effect of high energy radiation even at temperature as low as 130 K.[41] Unlike common semiconductors used today, for example GaN, Si, CdS, and GaAs, ZnO has a very high radiation hardness as well as strong optical and electical properties which make it a very promising semiconductor for research into space applications.[42, 43] The creation rate of vacancies due to radiation interactions is approximately 30 times lower than that of GaN.[5, 44] The same properties that make ZnO applicable as a semiconductor make it applicable as a scintillation detector for ionizing radiation, particularly charged particles.

CHAPTER 3
METHODOLOGY AND PROCEDURES

All chemicals used in this project were purchased through Sigma Aldrich, and chemical information and properties are available in Appendix A, Tables A.1 and A.2.

3.1 Substrate Selection

The first step in the project entailed selecting a substrate to grow the zinc oxide (ZnO) nanorods on. The selection was made purely on research done into weighing the different properties of the substrates as well as the cost per substrate. The key contributing characteristics that were taken into account are transmission percentage at 375-380 nm, surface energy, and cost. Surface tension of the contributing solvents used in the seeding experiment will also be discussed.

Many glass-type substrates such as fused silica, ITO glass, or quartz will not wet, which is to form a thin film of liquid across the surface of the glass, without the presence of an alcohol solvent. This can be seen in any rudimentary experiment with a drinking glass with water and a wine glass with wine. When the glass of water is poured out, the water will bead on the sides of the glass which shows its lack of ability to wet. Unlike water, alcohol has a very good wetting ability on glass as evidenced by the thin film or wet appearance after the wine is poured out. The reason for this is due to the surface tension of the liquid and the surface energy of the substrate [45]. The higher the surface tension of the liquid and the lower the surface energy of the substrate are, the higher probability a liquid will bead up.

In Table 3.1 and Table 3.2, the values for the surface tension and surface energy of solvents and substrates are given, respectively. The cost and transmission percentage at 375 nm of the substrates are also given in Table 3.2. Surface energy and surface tension are

Table 3.1: Surface Tension of Solvents [46, 47, 48]

Solvent	Surface Tension (dyne/cm at 20^o C)
Water (H_2O)	72.80
Ethanol (CH_3CH_2OH)	22.10
Methanol (CH_3OH)	22.70
Isopropanol ($(CH_3)_2CHOH$)	23.00
Monoethanolamine ($NH_2CH_2CH_2OH$)	48.30
Methoxyethanol ($CH_3OCH_2CH_2OH$)	30.84

Table 3.2: Surface Energy and Transmission Percentage of Substrates [49, 50, 51, 52]

Substrate	Surface Energy (mJ/m^2)	Transmission Percentage at 375nm	Cost per substrate ($)
Fused Silica	104	99%	9.50
ITO Glass	47.1	<70%	9.90
Quartz	400	93%	24.58

a driving force in ability to coat a material with a solution. In general, to coat a substrate a form of alcohol, whether ethanol or methanol, is used. The reason for this is the low surface tension in comparison to other solvents, for example water. The issue with many alcohols is the low vaporization point of the liquid, but this can be altered with additives such as monoethanolamine (MEA) which is a main contributor to the sol-gel process which will be further discussed in the next section. Surface energy of a solid in contrast to surface tension of a liquid needs to be high to facilitate coating. Surface energy is what attracts the liquid into a coat through bonds at the atomic level. The selection process of the substrate came down to transmission percentage at 375 nm and cost at a higher degree of importance than surface energy. Fused silica has the highest transmission percentage in UV and is the cheapest among substrates suitable for this experiment. The surface energy of quartz is higher and the transmission percentage does rival fused silica, but due to wanting to maximize the light reaching the PMT and reduce cost, fused silica was chosen.

3.2 Seeding Technique and Procedures

In order to grow a uniform vertical array of ZnO on a fused silica substrate or any other desired substrate, for example ITO or quartz, the initial seeding of the substrate proves to be one of the most important steps. The reason for this is because without a uniform secure seed layer covering the entire growth area, the nanorods will tend to form clusters with growth in multiple directions also known as nanoflowers. Nanoflowers and other structures formed as a result of nonuniform seeding reduce efficiency of electron transport within the crystal which is important to emission of scintillation light.[53] In general, there are four different methods for seeding a substrate that have been used in previous research conducted in this area: sputtering, physical vapor deposition, dip coating, and spin coating. The first two, sputtering and evaporation, were not conducted as these processes are expensive due to equipment involved and time.

Prior to seeding, the substrates were cleaned thoroughly. There are many methods to cleaning and preparing a substrate for seeding. A widely used one is the use of the an ultrasonic cleaner and a variety of cleaning agents.[24] The process used for cleaning and preparing the 50.8 mm fused silica substrates utilized a combination of a few different chemicals in an attempt to "rough" the surface to increase surface energy available for bonding of the seed solution as well as remove any manufacturing by-products on the surface. The substrates were cleaned with warm soapy water for 8 minutes and then subjected to the following in the ultrasonic cleaner for eleven minutes each: acetone, isopropanol, and DI water. This was repeated once.

The first part of the seeding experiment undertaken was a dip coating using prefabricated ZnO nanoparticles in the form of a powder purchased through Sigma Aldrich. The process began with a treatment layer of dodecane-thiol in ethanol. The substrate was treated with a solution of of 1% dodecane-thiol ($CH_3(CH_2)_{11}SH$) in ethanol through application using a scratch resistant foam applicator brush and then heated at 100^{o}C for 15 minutes.

The solution of dodecane-thiol in ethanol has been shown to improve seeding of different substrates, for example woven fibers and other glass like substrates creating a more even seed layer by applying the solution.[54, 55] Dodecane-thiol improves bonding of metal oxides, for example zinc oxide, by altering the surface of fused silica substrate to allow zinc oxide particles to readily bond to its surface. The thiol-groups functionalize the surface of the silica wafer as a method for binding medals and medal oxides such as zinc oxide to its surface.[55] Following the treatment, the substrates were suspended in a mixture of isopropanol and the prefabricated ZnO nanoparticles in the form of powder for 15 minutes while constantly being stirred using a magnetic stirrer. The substrate was then removed, gently washed with deionized water to remove any loosely bonded nanoparticles to prevent large buildup of loose seed crystals on the surface of the substrate, which would cause growth deformities and multi-axial growth patterns. The samples were then preheated at 150^oC in air for 15 minutes. This procedure of dipping was performed three times. Post annealing was done at 300^oC for 30 minutes in air.

The second part of the seeding experiment undertaken was using spin coating and a sol-gel process. An overview of the process of the sol-gel method is depicted in Figure 3.1 as well as the different techniques for the thin film deposition onto a substrate or the creation of a ceramic. The sol-gel seeding solution was prepared using a solution of 0.6M zinc acetate dihydrate $(C_4H_{10}O_6Zn)$ and 0.6M monoethanolamine (MEA).[24] The purpose of MEA is to stabilize the solution due to the low vaporization point of alcohol solvents. The solvents that were used as a variable in order to determine the best for this experiment were ethanol and methoxyethanol as used in [57] and [24], respectively. Both of these have been used in the preparation of solutions by other researchers. The solution was mixed at 60^o C for 2 hours and then allowed to age for 24 hours before being sealed.[24] The seed layer was developed similar to that of [24] with the variation being that the spin coating was done for 30 seconds at 3000 rpm. The reason for this is to allow for more of the solvent to evaporate yielding a stronger seed layer.[45] The amount of seed solution dispensed was

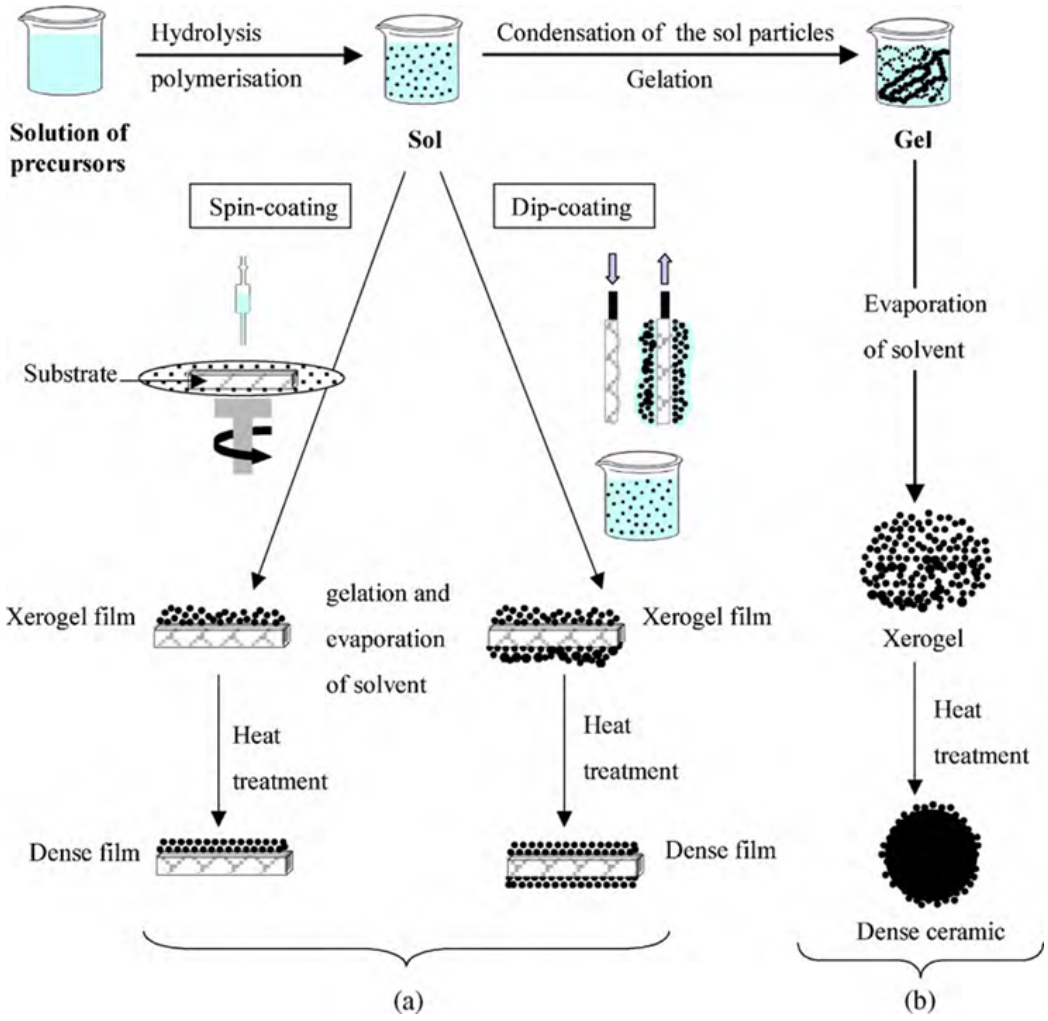

Figure 3.1: Overview of the sol-gel synthesis method: a) Thin films via colloidal solution; b) Ceramic formed from colloidal solution that has been transformed into a gel [56]

200 μL to allow for full surface coverage. The seed layer was then pre-heated at 250^{o}C for 10 minutes and then cooled to approximately 50^o C at a rate of 7-8^{o}C/min before being removed. This process was performed three times and then post-annealed at 550^{o}C for 1 hour in air.

3.3 Growth Technique and Procedures

A low temperature hydrothermal growth process was utilized as it is a low cost effective means of growing quality ZnO nanorods. The solution used to grow the nanorods consisted of 0.05M Zinc Nitrate Hexahydrate, 0.025M Hexamethyleneteramine (HMTA), 0.9M Am-

monia Hydroxide, .0012M Sodium Citrate, and the dopant whose concentration was varied. The reactions that generate the the ZnO nanorods was discussed in Section 2.3.2 Equations 2.9-2.16 as well as the role of each reactant in the generation.

This solution was put a glass jar and the seeded substrate was floated on top of the solution by wrapping the outer edge of the sample with teflon tape allowing for growth only on seeded side of the substrate. The jar was sealed with teflon tape and placed in a Yamato DKN400 Mechanical Convection Oven for 24 hours at 95^{o}C. Following growth, the jars were removed from the oven, and the samples removed. Each sample was thoroughly rinsed with DI water and then blown dry using a 10% Hydrogen-Nitrogen balance gas, which is the initial cleaning process used. Following characterization and attempt to detect ionizing radiation, it was discovered that there was most likely a large presence of quencher molecules bonded to the surface of the substrate resulting in the suppression of scintillation light. Following this discovery, a new cleaning method was introduced, and it consisted of high purity ethanol as a rinse using a steady stream followed by DI water and then repeated. After the rinse, the sample was thoroughly dried as before with a normal dry time of 3-4 minutes. This process was repeated once before further characterization was conducted with results being shown in the next chapter.

3.4 Characterization

3.4.1 SEM Structural and Atomic Analysis

In order to assess the structural shape, diameter, and length of the nanorods, the LEO 1530 Scanning Electron Microscope(SEM) with Energy Dispersion Spectroscopy(EDS) capability was used. Measurements were taken using the tool provided in the SEM program and confirmed using image analysis software, ImageJ. The purpose of SEM imaging is to verify uniform growth along one axis with even dense distribution before making any measurements or conducting spectroscopy. After verification of the physical characteristics, measurements of the diameter of several nanorods were taken and averaged as well as a

side angle of the sample viewed to take height measurements. A set up of the system as used in the laboratory is shown in Appendix A.

Atomic analysis of the samples to determine true percentage of dopant that was incorporated into the sample can be assessed through use of the EDS. The purpose of this is to better determine dopant concentration needed for future experiments into ZnO research such as nanocomposites and bulk melt. Later samples were not able to be analyzed using this feature of the SEM due to repairs needing to be made offsite, but would be benefitial to have the samples tested in the future to assess the actual dopant concentration in the crystals compared to that added to the growth solution.

3.4.2 Photo-luminescence Spectra

A photo-luminescence (PL) spectrum characterization is an optical characterization of a material that utilizes a laser to excite electrons across the band gap from the valence band to the conduction band to facilitate light photon emission as it returns to the valance band. Materials and compounds emit at different wavelengths and intensities and can be used to gauge the intensity of emission by a material when in the presence of radiation. The use of the laser is a non-destructive form of excitation where the use of radiation is a destructive form of excitation which can cause damage to crystalline structure over time through the creation of vacancies in the lattice structure.

Photo-luminescence spectra were obtained using a Kimmons IK5451R-E He-Cd dual wavelength laser with seven inches between shutter and sample as depicted in Figure 3.2. The wavelength used to excite the samples was the 325 nm with an output power of 10 mW. Spectra with the shutter open and closed were taken, averaged, and the background removed from the spectrum to yield the emission spectrum. A 325 nm Cuvette was used to filter out the 325 nm wavelength emitted by the laser. The signal from the fiber optic camera was processed through an Ocean Optics USB2000 Fiber Optic Spectrometer converting it to a digital signal.

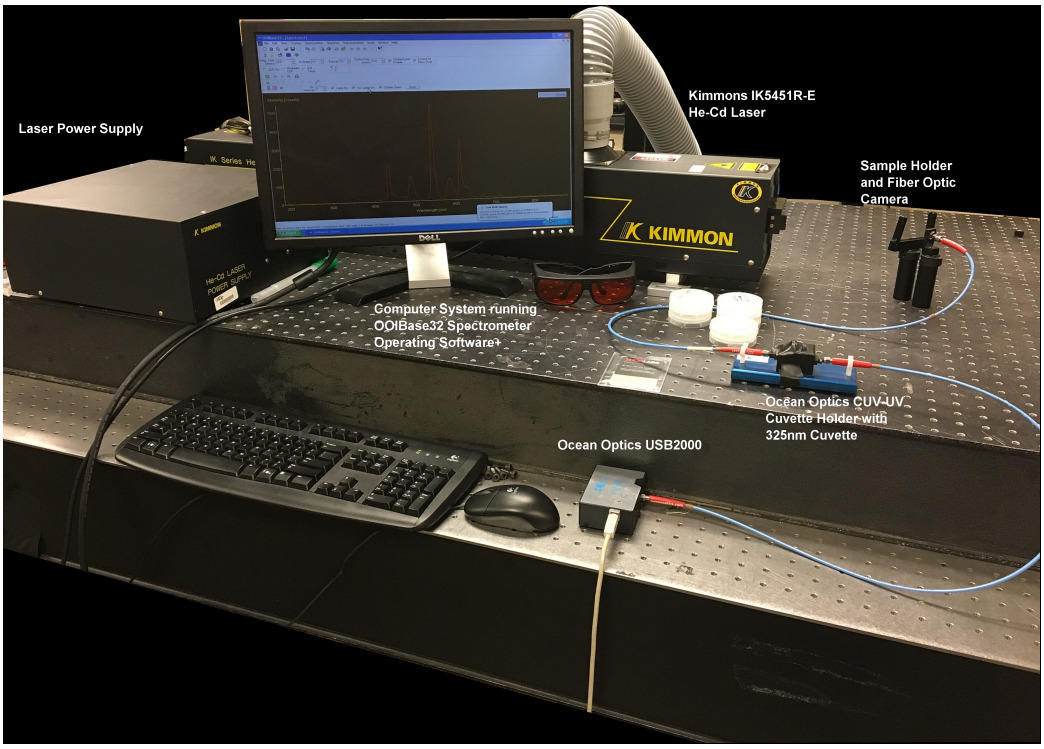

Figure 3.2: Photo-luminescence Spectra gathering Setup

3.5 Radiation Detection

The detection of ionizing radiation in the case of ZnO was focused on alpha particles, but through the inclusion of ^{6}Li or ^{10}B, neutrons can be detected because of the secondary charged particle produced from the reactions between the absorbers and the neutrons. The secondary particle of these elements is an alpha particle, which is where the radiation detection of this project is focused. Due to the range and mean free path of a 5.5 MeV alpha particle being small compared to other radiation in like media, approximately 3.5 cm and 15.43 μm in air and ZnO, respectively, the energy of the alpha particle will change a great deal over small changes in distance from the detector.[7, 9, 59, 58] With the use of a thin film as a detector with an approximate of 2-3 μm, the projected range of the alpha particles is larger than that of the detector as shown in Table 3.3. In this experiment, the source distance from the detector was varied from 1.0 cm to 2.5 cm with incremental distance changes at 1.5 and 2.5 cm. The setup utilized a light proof box, NIM bin, and computer

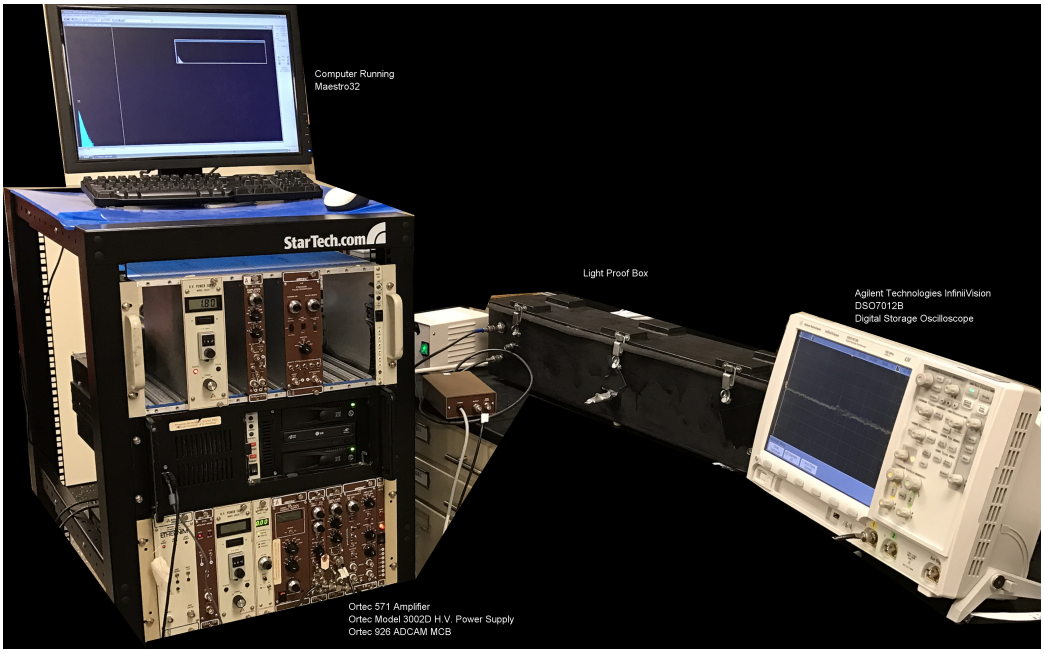

Figure 3.3: Radiation Detection Setup Overview

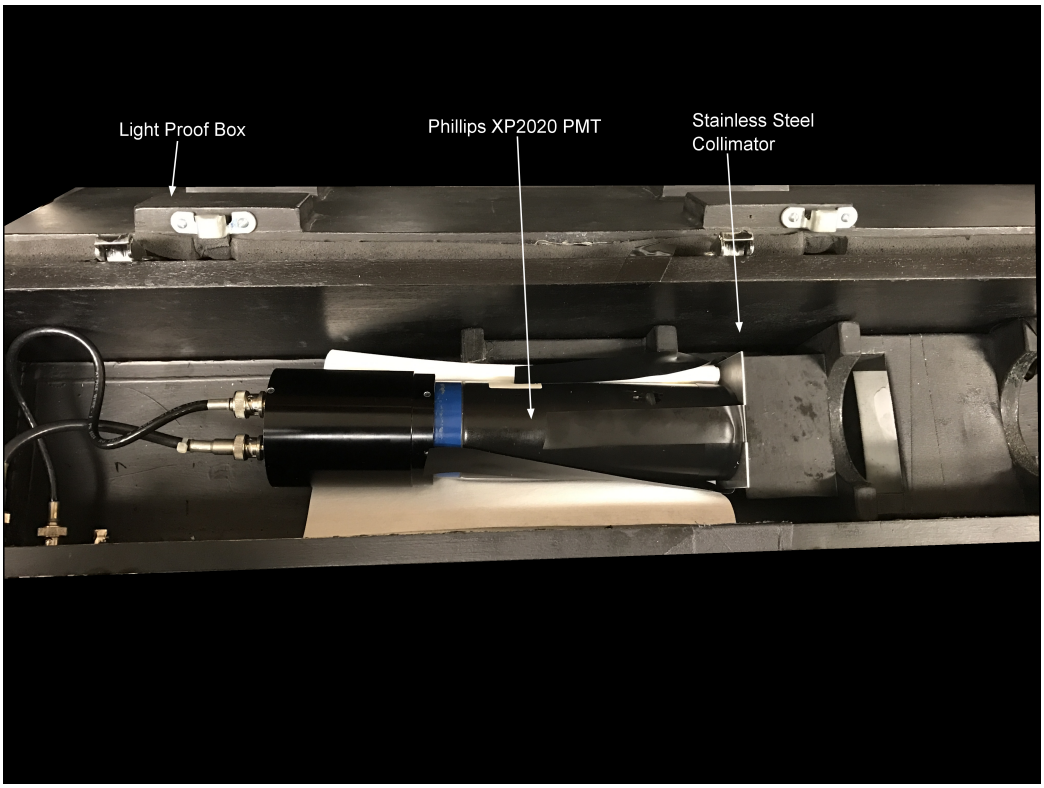

Figure 3.4: Light Proof Box Setup

Table 3.3: Projected Range of α-particles in ZnO[58]

Ion Energy (MeV)	Projected Range (μm)
0.100	0.439
0.500	1.440
1.000	2.450
1.500	3.500
2.000	4.620
2.500	5.850
3.000	7.170
3.500	8.610
4.000	10.15
4.500	11.80
5.000	13.56
5.500	15.43

consol. In the light proof box, a Phillips X2020 photo multiplier tube with the detector coupled to it using silicon optical grease and a collumator with a 3 mm diameter hole drilled attached 0.5 cm from the surface of the detector. Cables were run from the light proof box to an Ortec 113 preamplifier which connected to equipment in the NIM bin. The equipment powered by the NIM bin included an Ortec 572 Amplifier, an Ortec 926 ADCAM MCB, and an Ortec Model 3002D High Voltage Power Supply used to power the PMT. The MCB converts the analog signal received from the amplifier to a digital signal read by the computer running Maestro, which is a software developed by Ortec. The overall and light proof box setups can be seen in Figures 3.3 and 3.4. The purpose of the collumater was to shield out alpha particles that had an angle of incidence outside of that which would put it inside of the hole which will produce a better photo peak at the cost of count rate. Due to the decreased count rate, spectra were taken over 3 hours.

The ultimate goal for the research into ZnO as a radiation detector is the detection of neutrons. Neutron detection, though outside of the scope of this project, is discussed in Chapter 6.

CHAPTER 4
RESULTS AND ANALYSIS

Due to the broad scope of the project and the multiple avenues of analysis taken in order to develop the best baseline for future work with respect to seeding, growth, and characterization, optimization will require more in-depth experimentation and analysis in the future to determine the functionality of a zinc oxide nanorod detector. In this chapter, a look at seeding techniques, crystal/nanorod characterization, photo-luminescence spectra, and α-particle radiation detection ability are discussed. The purpose of the multiple areas of analysis and data collection is to provide the best baseline possible in ZnO nanorod radiation detectors for future work to be conducted in refining and optimizing the detector to determine viability for commercialization as a radiation detector. Future work into this specific type of detector will be discussed further in Chapter 6.

4.1 Comparison of Seeding Technique

To achieve uniform growth along the vertical axis perpendicular to the substrate, the seeding of the substrate is very important. Without a uniform seed layer that covers the entire surface of the substrate, there will be alternate crystal formation, for example nanoflowers and nanoclusters. These formations create a less efficient structure with respect to electron mobility as the electron has to cross crystal boundaries in some instances or traverse abnormal formations to find a site to return to the valence band. Of the forms of seeding as discussed in Section 3.2: Seeding Techniques and Procedures, dip coating and spin coating were chosen due to cost, equipment availability and time.

The first process, dip coating, utilizes prefabricated nanoparticles in the form of a powder, which was added to isopropanol to make a colloidal mixture. As can be seen in Figure 4.1a, the seeding of the substrate produced a non-uniform and incomplete seed layer

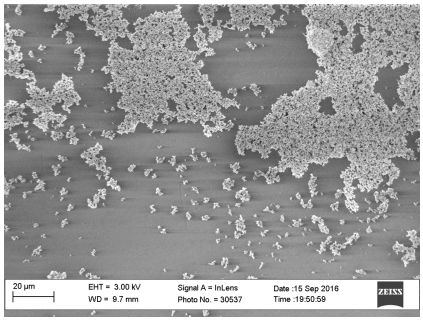

(a) Seed Layer

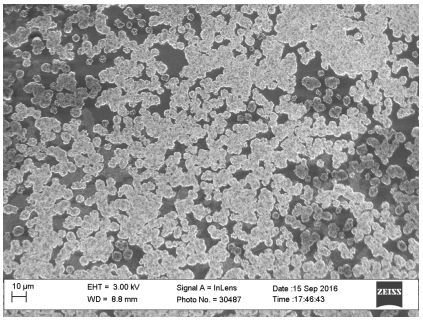

(b) Overview Image of Nanorods

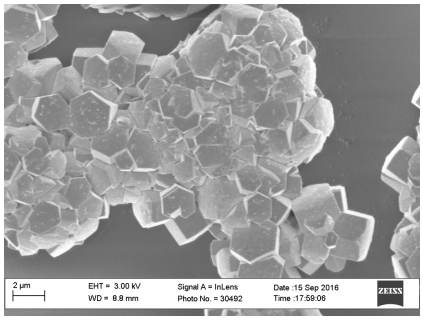

(c) Magnified Image of Nanorods

Figure 4.1: Seed Experiment 1 Results from Seed to Growth

with large gaps of substrate that did not accept a seed layer. Due to the non-uniform and incomplete seed layer, the formation of nanoflowers and nanoclusters occurred. These formations do not adequately cover the surface of the substrate as shown in Figures 4.1b and 4.1c; therefore, due to both non-uniform and incomplete growth across the surface of the substrate, the dip coating process was determined to be ineffective for this work in the development as a radiation detector. Without complete coverage and a uniform growth, detection ability will not be optimized and create gaps in coverage across the detector as well as incomplete and uneven energy transfer. Also, the formation of clusters and nanoflowers degrades the efficiency of electron transport within the crystal structure which will effect radiation detection as electron/hole pairs migrate to luminescence sites.[60, 61] The reason for this is that the migration of electron/hole pairs has very high mobility within crystalline structure of ZnO, but very poor with respect to movement between crystals. Therefore, vertically aligned nanorods will have the best mobility and transport to recombination sites.[61] The incomplete coverage was verified using energy dispersive spectroscopy and

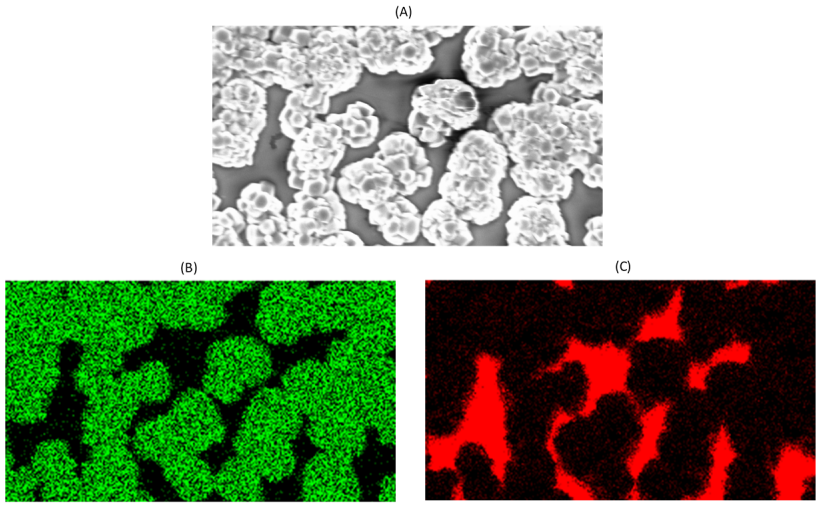

Figure 4.2: Incomplete coverage of substrate confirmation through Energy Dispersive Spectrocscopy: (A) SEM Image analyzed, (B) Zinc, and (C) Silicon

can be seen in Figure 4.2. The empty space seen on SEM pictures was confirmed to be silicon which confirms the incomplete growth across the substrate.

Dodecane-thiol concentration was varied in order to ascertain if an increased presence of thiol groups available to functionalize the fused silica molecules would enhance the ability of the nanoparticles to bond to the surface. There was no change to the overall seed layer formed on the surface of the substrate by increasing the concentration of dodecane-thiol; therefore, while the dodecane-thiol treatment did increase the ability for nanoparticle to bond to the surface, it was not a great enough effect as to ensure a uniform seed layer covering the entire surface. This led to the conclusion that seed experiment one should not be used for this project.

The second process investigated involved the use of a spin coater to deposit a layer of ZnO. Using the same process as described in [24], the same results with respect to clearly defined crystalline shape of the seed layer were not achieved but did yield uniform coverage containing the needed elements to form a seed layer to produce a vertically aligned, dense nanorod array. Though the actual cause is not able to be determined at this time, the alteration of the substrate may have resulted in less crystalline form of the seed layer or use of standard convection oven instead of furnace resulted in a less ideal heating environment.

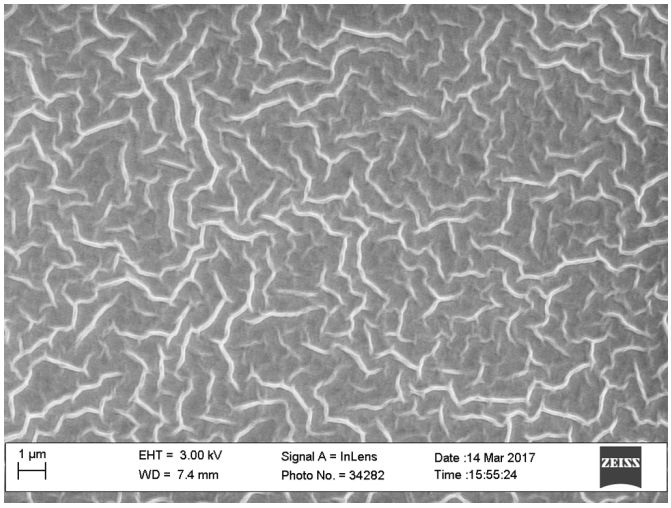

(a) Seed Layer for Seed Experiment 2

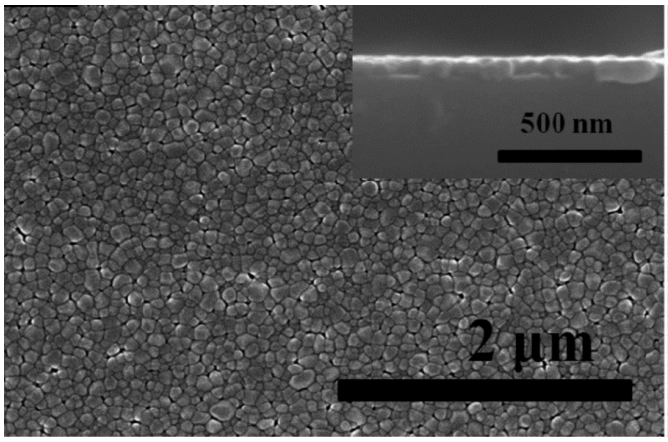

(b) Seed Layer from [24]

Figure 4.3: (a)Results of seed deposition using method in [24] and (b)Results achieved in [24]

Further analysis and experimentation into this seeding technique is needed on fused silica as there was not a published paper discovered that covered a preferred seeding techniques for fused silica with ZnO and how to achieve optimal results. This will be further discussed in Chapter 6. As can be seen in Figure 4.3a, the seed layer due to spin coating covers the entire surface of the substrate, and though crystalline layer was not achieved, it provided a better layer to grow uniform nanorods along one axis then the first seed experiment as shown in the next section. The seed layer appears as though it starts to form crystalline structures which with additional heating procedures could form the seed layer as seen in

Figure 4.3b.[24] Due to the full coverage of the substrate formed by using spin coating, it was determined that at this point, unless access to the various other means such as evaporation deposition or sputtering is available, spin coating is the more cost effective means of depositing a seed layer that covers the entire face of the substrate. For the remainder of the experimental results and discussion chapter, the spin coating seed technique was used to achieve the results shown.

4.2 Scanning Electron Microscope (SEM) Characterization

Characterization of the nanorods of both undoped and doped samples was undertaken to view the crystalline structure as well as see the effects of the dopants on the overall growth mechanisms as seen from the dimensions of the nanorods (height and width) in 4.1. Characterization of the crystalline structure is needed in order to ensure that no crystalline off-chutes were formed off of the face of the nanorods. Off-chutes or splintering crystals occur due to non-uniform growth and seeding and effects have been seen when different annealing atmospheres were used during the first seed experiment as seen in Figure 4.4. If the seed research reaches the point where annealing can be performed, then an alternate atmosphere such as pure hydrogen, hydrogen/nitrogen mix (normally 10%, balance nitrogen), or hydrogen/argon (normally 10%, balance argon) are choices that could be used. In order to obtain length measurements, the samples were broken in half using a glass cutter and analyzed. There was little variation from the middle of the substrate to the edge of the growth region which is promising and shows uniform growth of the nanorods across the face. Length of the nanorods is important because due to the nature of thin film detectors. Many times, the range in matter of ionizing radiation exceeds that of the detection area and ZnO nanorod detectors are no exception. Studies into achieving long nanorods of a length of fifteen to sixteen micrometers is work to be performed in future research while also keeping width of nanorods for improved electron transport. The reason for needing a length of fifteen to sixteen micrometers is due to the range in ZnO of a 5.5 MeV alpha

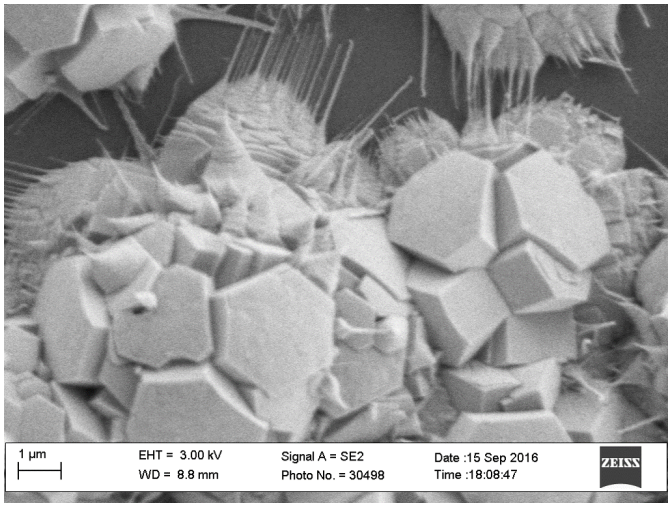

(a)

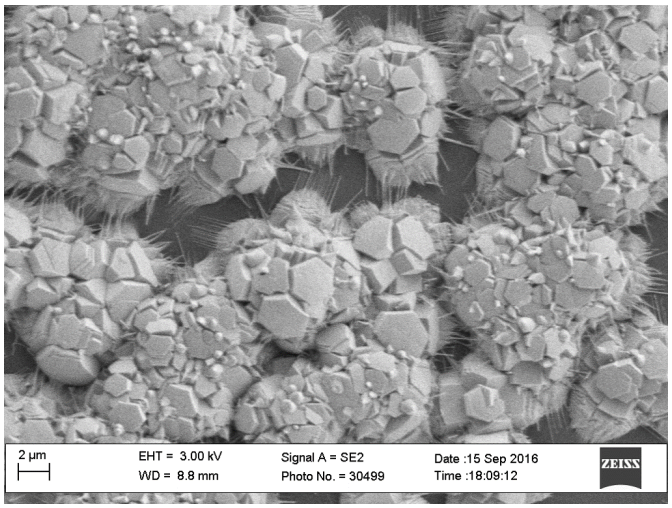

(b)

Figure 4.4: Off chutes and splintering causted by annealing in air rather then atmosphere void of oxygen

particle (^{241}Am emission) is approximately 15.4 μm as shown in Table 3.3.

To compare how the dopant as well as dopant concentration effects the growth and morphology of the crystal structure, they will be compared to an undoped sample grown and tested under the same condition. SEM images showing the dense full coverage of the substrate, a magnified view of the nanorods used to take measurements of the width, and an image taken from the broken side of the substrate to record height for various dopants and dopant concentrations are shown in Figures 4.5, 4.6, 4.7, 4.8, and 4.9. Based off of

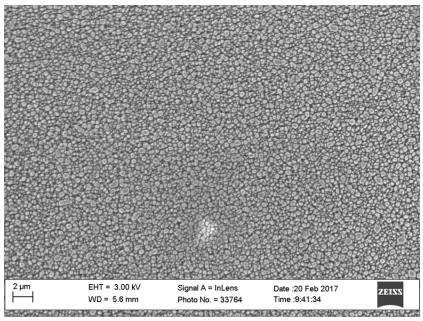

(a) ZnO Undoped Overview

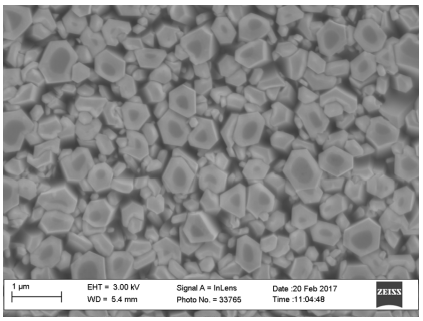

(b) ZnO Undoped Magnified

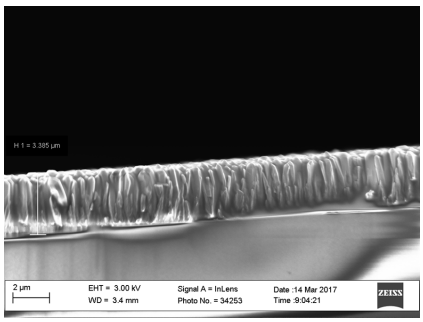

(c) ZnO Undoped Side Height Measurement

Figure 4.5: Scanning Electron Microscope (SEM) images of undoped sample of ZnO

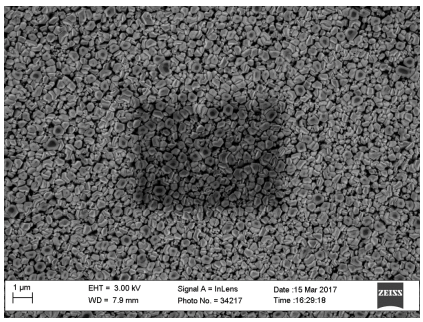

(a) ZnO:Ga 1.0% Overview

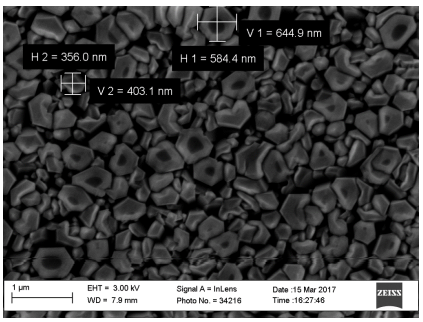

(b) ZnO:Ga 1.0% Magnified

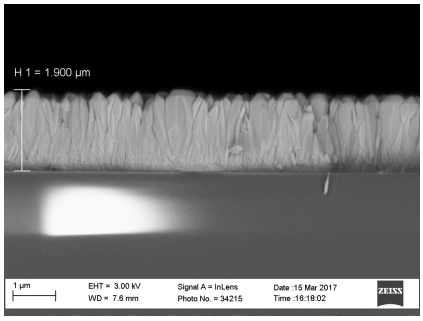

(c) ZnO:Ga 1.0% Side Height Measurement

Figure 4.6: Scanning Electron Microscope (SEM) images of ZnO:Ga 1.0%

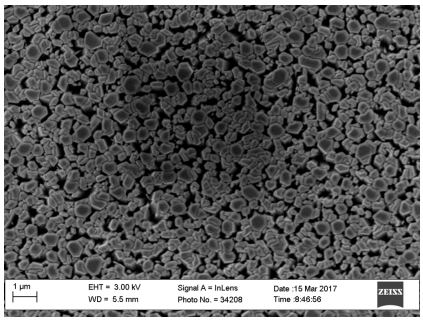

(a) ZnO:Ga 0.5% Overview

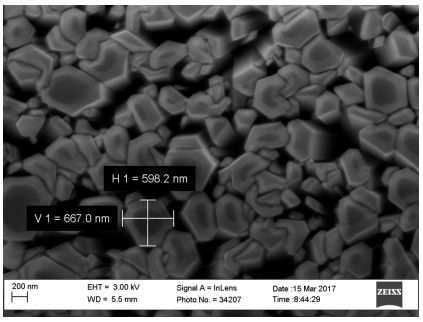

(b) ZnO:Ga 0.5% Magnified

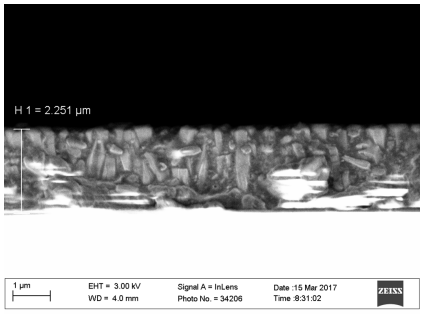

(c) ZnO:Ga 0.5% Side Height Measurement

Figure 4.7: Scanning Electron Microscope (SEM) images of ZnO:Ga 0.5%

Table 4.1: Measurements of Nanorods from SEM Images

Sample	Length (μm)	Width Measurements (nm)
ZnO Undoped	3.385	669.3x780.5
ZnO:In 1.0%	2.542	411.2x473.2
ZnO:In 0.5%	2.130	621.8x559.6
ZnO:Ga 1.0%	1.900	644.9x584.4
ZnO:Ga 0.5%	2.251	667.0x598.2

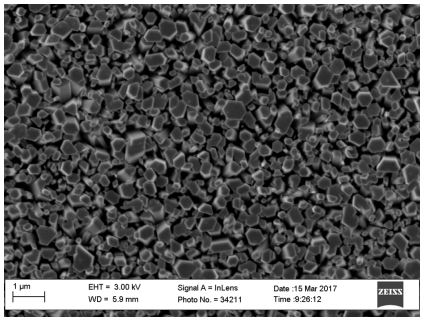

(a) ZnO:In 1.0% Overview

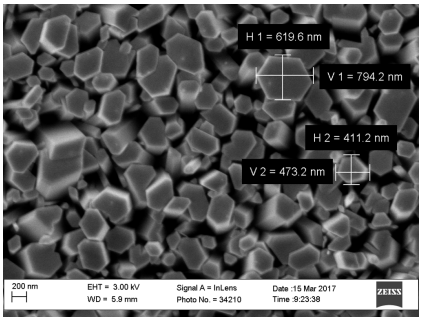

(b) ZnO:In 1.0% Magnified

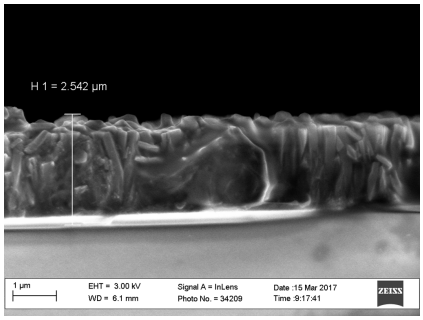

(c) ZnO:In 1.0% Side Height Measurement

Figure 4.8: Scanning Electron Microscope (SEM) images of ZnO:In 1.0%

previous research performed at higher dopant concentrations of the dopants used, there was a preconceived notion of what the comparison for each dopant would look like compared to undoped.[24, 62] Gallium reduces the length to a large extent and has small effect on the width as well as gives poor overall crystal structure and indium generally reduces the length slightly and the width is narrower than that of undoped.[24]

As can be seen in Table 4.1, the generalizations stated above for the most part held true. Further analysis over larger areas of the samples to give a true average is needed to truly confirm effects of dopant and dopant concentration, but with analysis conducted, the results fall in line with notions conceived through literature. With indium doped nanorods, as expected, the length reduces approximately 800 nm and the width measurements reduce 200-300 nm which is in line with previous results and research with the shortening and narrowing of the nanorods. When the concentration of indium was reduced, the width measurements increase as would be expected as the nanorods get closer to the undoped growth mechanism, but the length decreased which could result from several factors such

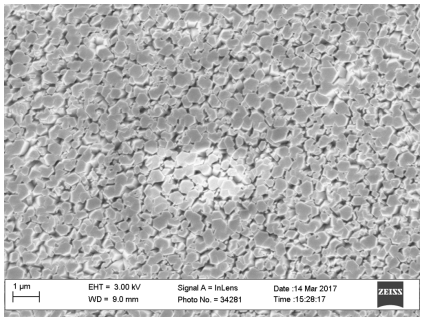

(a) ZnO:In 0.5% Overview

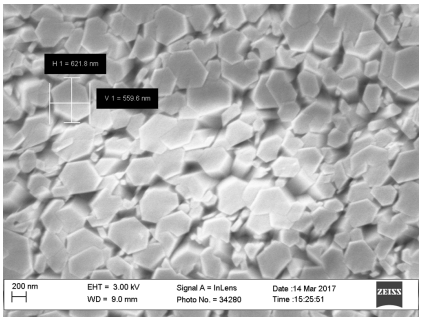

(b) ZnO:In 0.5% Magnified

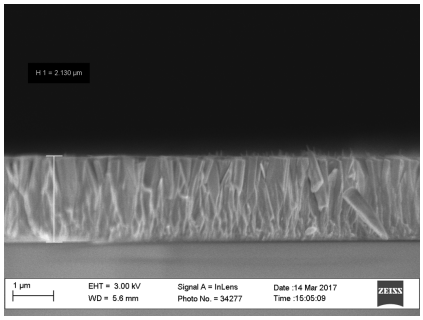

(c) ZnO:In 0.5% Side Height Measurement

Figure 4.9: Scanning Electron Microscope (SEM) images of ZnO:In 0.5%

as citrate interaction shift more to the Zn^{2+} ion. At higher dopant concentrations, citrate anions might be largely taken up by dopant ions allowing more availability of Zn^{2+} for vertical growth. Dopant ions have a higher positive charge, In^{3+} and Ga^{3+} compared to Zn^{2+}; therefore, the ions would have a higher attraction to the citrate anions. Several reasons are possible such as the length measurement taken is not a true length and is on the shorter end which would be verified through more in-depth analysis and measurements or perhaps the decreased length is due to a morphology change of the crystal due to a decreased concentration of defect. A change in placement of dopant ion within the crystal effects many things such as bond lengths and shape and any of these rationale could be the cause. Theoretical analysis has not be performed for ZnO:In with respect to effects caused by ion replacement versus interstitial placement of dopant ion and could be analyzed in the future. With respect to ZnO:Ga the results are as expected for the 1.0% and 0.5%. There was a great decrease in length (1.0+ μm) as seen in previous research literature with an overall crystalline degradation. The reasons for the vast difference between the two dopants

even though in same elemental group in the crystalline structure and shape is unknown at this time and not present in research done in literature review.

4.3 Photo-luminescence Spectra

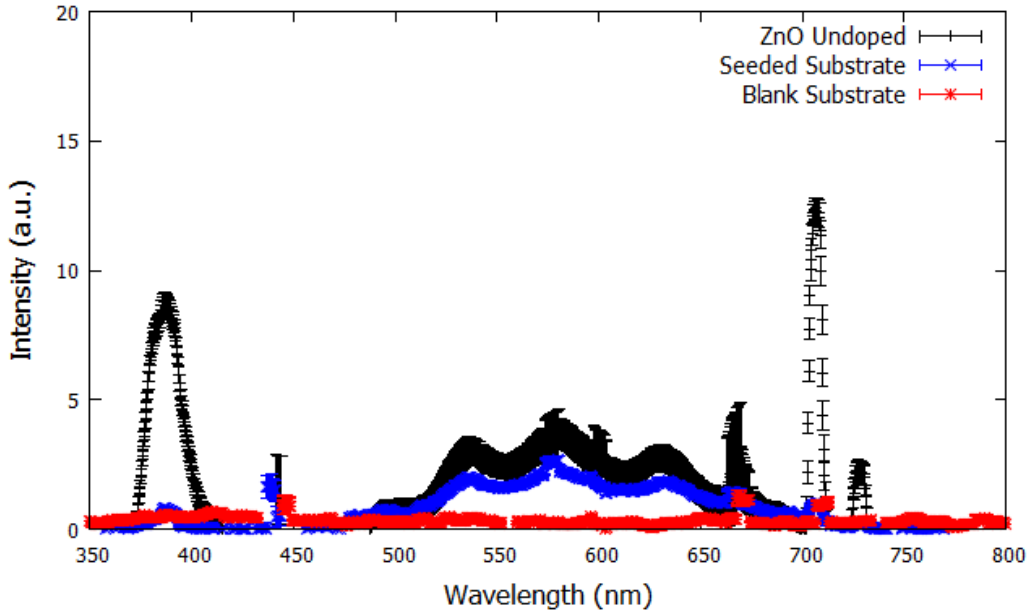

Figure 4.10: Photo-luminescence Spectra of Undoped ZnO, Seeded Substrate, and Blank Substrate

Photo-luminescence spectra verify band-edge emission (approximately 380 nm) and lower energy, broader emission in the visible spectrum were taken of all samples as well as a seeded sample and blank substrate. The purpose of taking spectra of the seeded and blank substrates was to note any effects that they may have on the overall emission by the samples of grown nanorods. The emission spectra of the blank and seeded substrates compared to the undoped emission spectra can be seen in Figure 4.10. As expected, there was little emission by the blank substrate as the transmission percentage for wavelength of the laser is almost 100%. The little absorbed by the substrate shows a minor emissions consistent with emission spectrum of elemental oxygen and silicon, both present in fused silica (SiO_2). Elemental spectrums can only explain parts of the emission spectrum as the addition of bonds and their respective bond lengths also greatly affect the emission of a

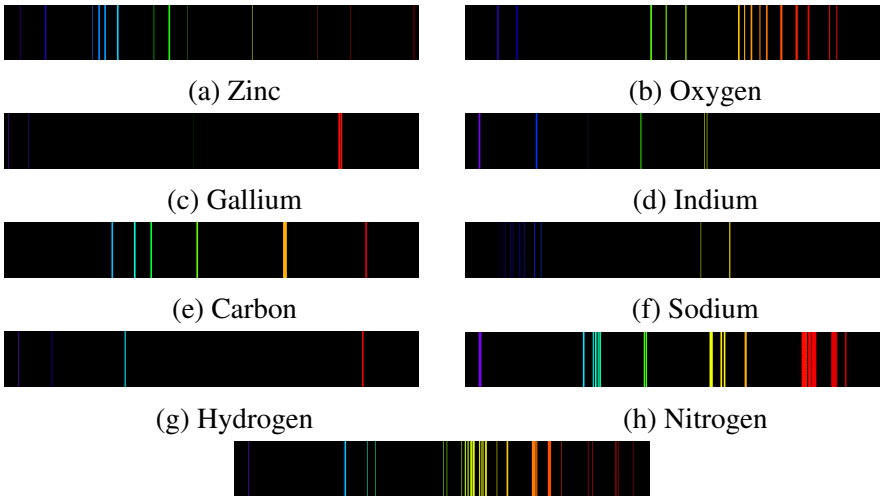

Figure 4.11: Emission Spectra for various elements present in Seed and Growth Solutions and the Substrate.

molecule or crystal. The seeded spectrum shows a very strong emission in the broad emission area of the undoped ZnO sample. The transmission percentage of 325 nm wavelength used for excitation is near zero and will be absorbed within the length of the sample mostly near the surface of the nanorods; therefore, the broad emission of the grown sample cannot be directly assigned to the seed layer. The broad emission has been analyzed and discussed since the research into ZnO began in the early to mid-twentieth century. One school of thought is that the broad emission is caused by impurities within the ZnO nanorod structure and based off of the emission of the seed layer this would trend towards that hypothesis. Other researchers have assigned the broad emission to oxygen vacancies within the lattice structure but without more in-depth analysis of the seed layer itself neither hypothesis can be verified for this instance.[28] Further explanation is available in Section 2.3.1 as to the cause of the broad emission and the contradiction and disagreement between researchers. Since defined hexagonal crystalline seeds were not formed, there are most likely impurities from the other elements that make up the seed solution that were not completely evaporated and removed during pre- and post-heating processes. Without fully formed crystilline structure, vacancies within the loosely formed strutures are plausible.

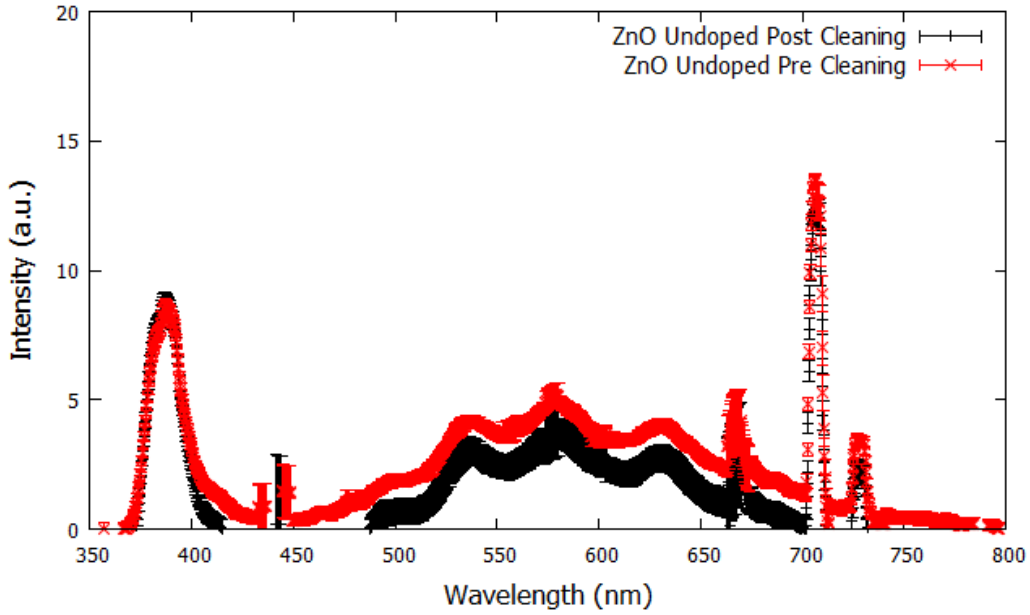

Figure 4.12: Photo-luminescence Spectra of Undoped ZnO Pre- and Post-Cleaning Method

Due to the poor scintillation detection of ionizing radiation, which will be further explain later in this chapter, a new post growth washing technique was implemented as written in Section 3.3. The reason for this is due to quenching atoms, ions and molecules bonded to the surface of the crystal. Normally, these are removed through an annealing process, but due to inability to anneal as previously discussed they needed a more extensive washing procedure. The new washing had some effect on the photo-luminescence spectrum of undoped ZnO as peaks became more defined and the broad emission was slightly reduced as seen in Figure 4.12. The band edge emission was unaffected with only a minor increase in intensity with the cleaning method, but as will be shown in the radiation detection portion of the this chapter, the effect of the cleaning was significant which trends towards the belief to some extent that a large presence of quenching molecules bonded to the surface of the crystals.

The photo-luminescence spectra of both indium and gallium are shown in Figures 4.13 and 4.14 respectively and then compared according to dopant concentration of 1.0% and 0.5% in Figures 4.15 and 4.16 respectively. With the exception of ZnO:In 1.0%, the in-

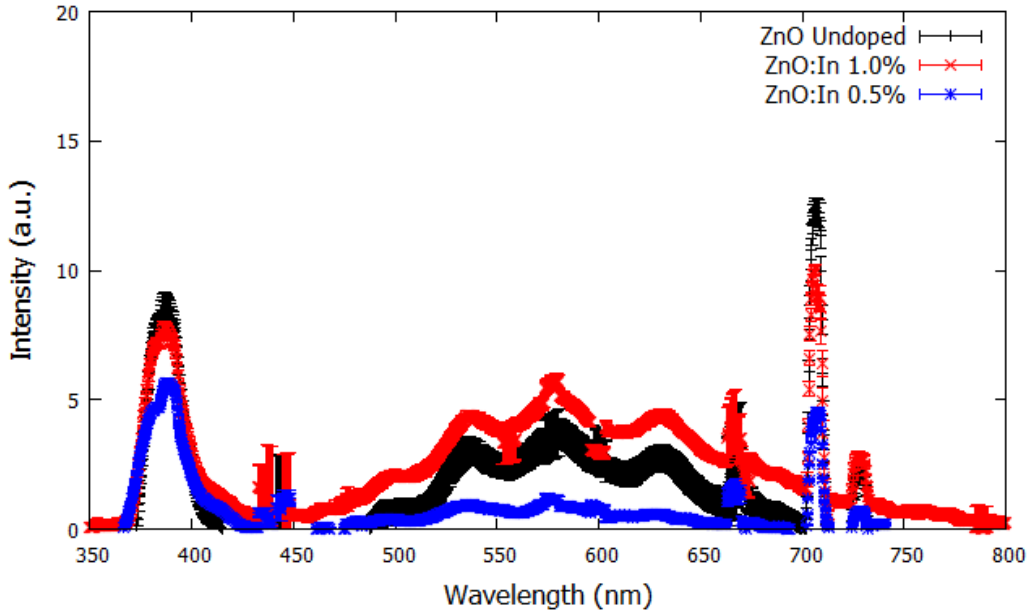

Figure 4.13: Photo-luminescence Spectra for ZnO and ZnO:In samples at 1.0% and 0.5%

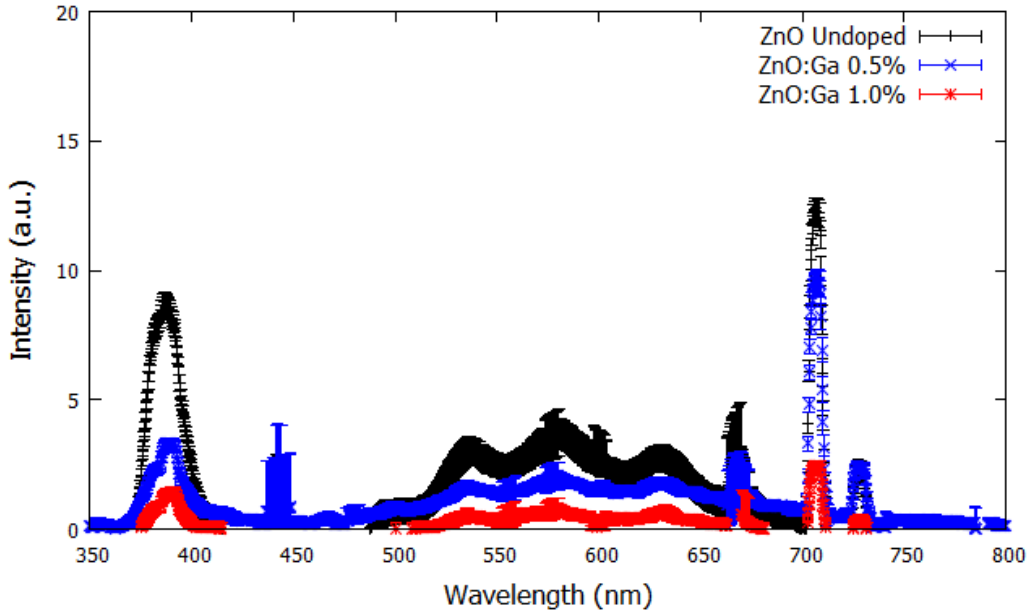

Figure 4.14: Photo-luminescence Spectra for ZnO and ZnO:Ga samples at 1.0% and 0.5%

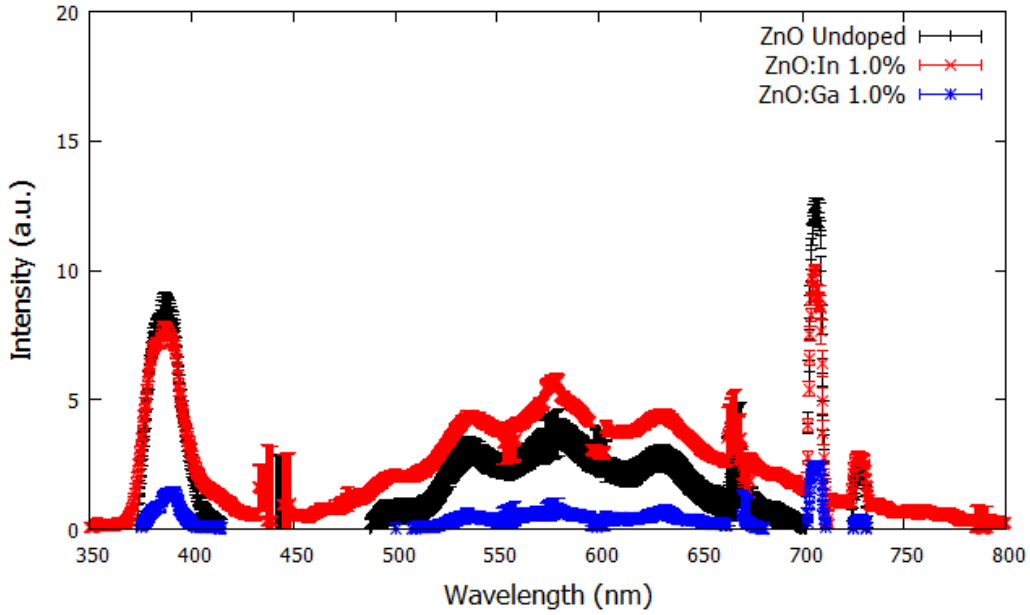

Figure 4.15: Photo-luminescence Spectra for ZnO and 1.0% doped samples of In and Ga

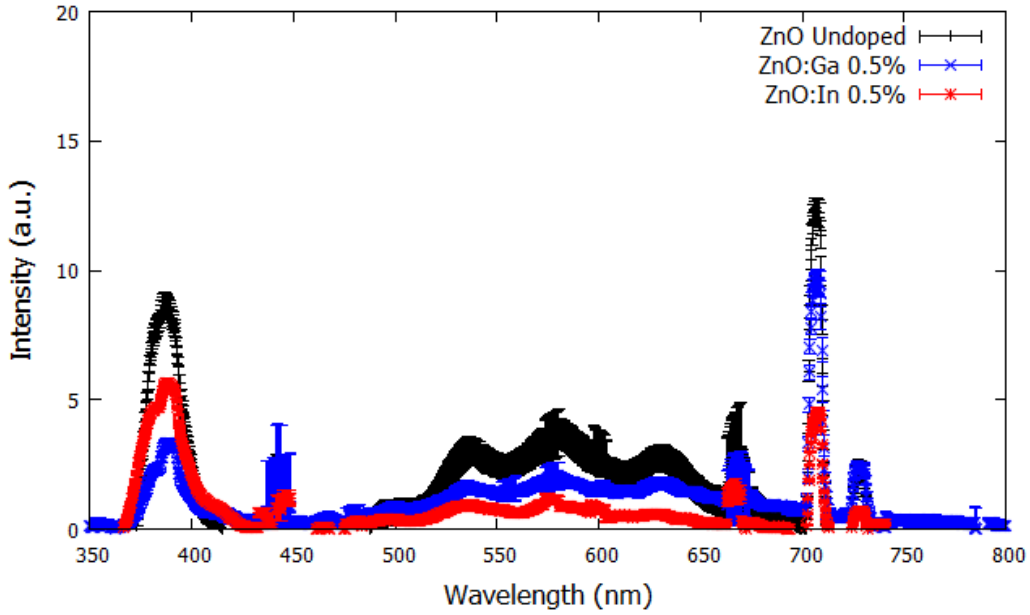

Figure 4.16: Photo-luminescence Spectra for ZnO and 0.5% doped samples of In and Ga

clusion of gallium and indium affected the PL spectra in line with the thought that the broad emission is due to zinc vacancies and that the inclusion of dopants such as indium and gallium decreases the number of zinc vacancies as they would take the place of the vacant zinc in these positions. By decreasing the zinc vacancies, the broad emission is suppressed to some extent but also effects the near band edge emission as discussed in Section 2.3.1. With the inclusion of dopants the shift in absorption and transmission band, there will be degradation in the emission spectra. The contradiction throughout literature as to the cause of the broad emission prevents precise explanation as the effects of the dopants on the photo-luminescence spectra. The conclusions that can be drawn from the spectra are that the inclusion of gallium and indium do have an effect on the emission properties and intensities in comparison to undoped ZnO and that the change in dopant concentration again alters the spectra. Whether the concentration effects placement within the crystal such as interstitial and lattice substitution cannot be confirmed; however, there has been theoretical research into the effects of such placement on the photo-luminescence and absorbance spectra with respect to gallium doping in ZnO as shown in Section 2.3.1. From previous research, the interstitial placement of gallium is the cause for the degredation of the emission spectra.[34] The emission spectra for gallium doped samples shows that substitutional placement is preferred due to improvement of emission spectra with decreasing concentration.

4.4 α-particle Detection

The next area of emphasis was to test the ZnO nanorods as radiation detectors against an alpha emitter, ^{241}Am. Due to the size of the detector surface area and volume, approximately 20.27 cm^2 and .0051 cm^3, respectively, using 2.5 μm nanorod length and 2.54 cm radius, the effectiveness for ionizing radiation such as neutrons and gamma is essentially zero and limited at best. For heavy charged particles, for example alpha particles, that have a high linear energy transfer (LET), the detectability using thin film detectors increases. Because

the range of an alpha particle in ZnO is greater than the length or thickness of the nanorod detector, the full energy is not deposited by alpha particles interacting with the detector. In the next section, a theoretical approach to determine energy deposited was taken depending on energy entering the detector which was attenuated by increased distance of source from the detector. Physical experiments were done by varying the distance from the detector for undoped ZnO and also comparing spectra results for 2.50 cm source distance from detector for doped samples. For a detector such as a thin film, the presence of even small amounts of quencher molecules have a significant effect compared to that of normal detectors.

4.4.1 Theoretical Simulations using SRIM/TRIM

Table 4.2: Transmission of 5.5 MeV α-particles through Air

Distance from Detector (cm)	Transmission Percentage (%)	Average Energy (MeV)
1.00	99.999	4.583
1.50	99.997	4.074
2.50	99.990	2.902

The theoretical approach taken was to determine average energy deposited in the sample by one million particles in order to better evaluate the experimental data obtained. Using the TRIM function of SRIM, one million particles were passed through air at the distances of 1.0 cm, 1.5 cm, and 2.5 cm in order to obtain the transmission data and average energy of the alpha particles entering the detector. This data is displayed in Table 4.2. Those energies were then simulated using TRIM to find the average energy deposited in ZnO by one million particles. Past 2.50 cm the alpha particles begin to enter the Bragg peak region of their energy loss, which SRIM does not simulate and will not produce reliable results. Once the particles are into that region the energy of the particles entering the detector will vary greatly; therefore, in the interest to get as clear a peak as possible and study the results the distance was not varied past 2.50 cm. The density of ZnO was kept constant at 5.61 g/cm^3 for all samples run with stoichiometric percentages for dopants according to that of

what was used (1.0% and 0.5%). Dopants will alter lattice constants, but without a way to measure the lattice constants of the experimental samples, the lattice constants were held constant.

Table 4.3: Energy Transfer of α-Particle in undoped ZnO

α-Particle Energy (MeV)	Average Energy of Particles Transmitted (MeV)	Average Energy Transferred in Detector (MeV)	Minimum energy Transferred (MeV)	Maximum Energy Transferred (MeV)
4.583	3.54	1.04	0.938	4.35
4.074	2.95	1.13	1.02	3.93
2.902	1.52	1.38	1.27	2.86

Simulations to obtain average energy transfer from the α-particles entering the detector were conducted for the various energies obtained in Table 4.2 for undoped ZnO nanorods with a length of 3.385 μm from measurement obtained in SEM characterization listed in Table 4.1. The average energy of the particles transmitted through the detector and the energy transferred from the particles are listed in Table 4.3. As the energy decreased for alphas entering the detector, the average energy transferred increased as expected due to the stopping power of the ZnO increasing as the alpha energy decreased. The number of full energy depositions increased as well from seven particles being fully absorbed to thirty-three. Based off of the maximum and minimum energy of particles transmitted compared to the average energy, the distribution of energy of the particles is a right biased distribution with respected to the transmitted particles energy. The minimum and maximum values for the particles are given in Table 4.3. Alpha particles passed through ZnO doped with gallium and indium at the dopant concentrations of 1.0% and 0.5% were simulated in a similar manner to the undoped at an alpha particle energy of 2.902 MeV. The results of the simulations are listed in Table 4.4. Energy transfer does not necessarily translate directly to excitations and light photon emissions as the mechanism and migration to a luminescence center and how dopants effect this mechanism are not the same. Generally, the longer the

nanorods; the more energy transferred; the more likely to have strong light photon output given minimal quenching sites.

If it takes approximately three times the band gap to create one electron-hole pair as discussed in Section 2.2.1[9], the average number of electron excitements per alpha particle is approximately 140,000 for initial alpha particle energy of 2.902 MeV based off of band gap of approximately 3.3 eV. Of the 140,000 pairs produced with photon emission close to 100% for electron-hole production, approximately 140,000 light photons will also be produced. Using fractions for ZnO and fused silica calculated in Table 2.1 in Section 2.2.2, the number of light photons will be significantly reduced. Of the 140,000 light photons, using values calculated from [14], approximately only an eigth to a quarter of the photons will reach the PMT. This value can be increased in manufacturing as an inner surface will surround the detector reflecting the half of the photons that escape the top of the nanorods.[8]

Table 4.4: Energy Transfer of 2.902 MeV α-Particle in ZnO:In and ZnO:Ga at 1.0% and 0.5%

Sample	Average Energy of Particles Transmitted (MeV)	Average Energy Transferred in Detector (MeV)	Minimum energy Transferred (MeV)	Maximum Energy Transferred (MeV)
ZnO:In 1.0%	1.90	0.999	0.907	2.89
ZnO:In 0.5%	2.07	0.828	0.739	2.81
ZnO:Ga 1.0%	2.17	0.733	0.658	2.90
ZnO:Ga 0.5%	2.02	0.879	0.79	2.86

4.4.2 Experimental Analysis

Due to initial results with respect to radiation detection, an intensive cleaning method was applied. This cleaning was due to the proposition of the presence of quenching molecules bonded to the surface of the nanorods resulting in more quenching sites readily available for excited electrons. Due to a large presence of oxygen in by products of the synthesis

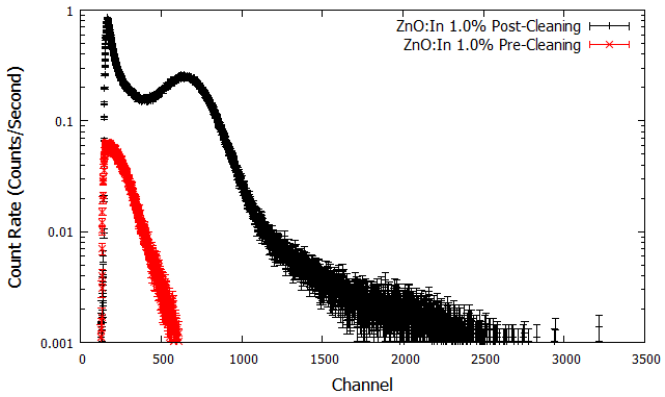

(a) ZnO:In 1.0%

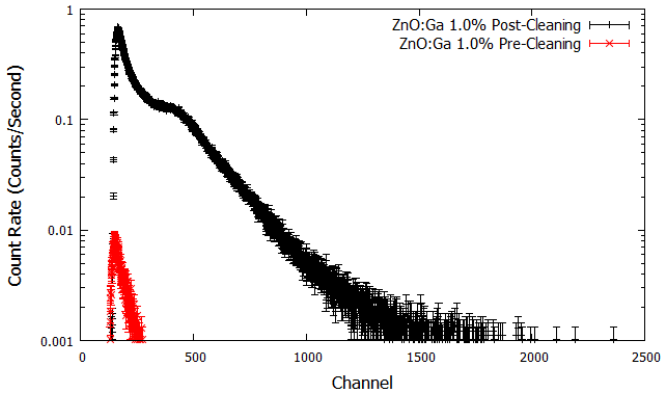

(b) ZnO:Ga 1.0%

Figure 4.17: ^{241}Am Spectra at 2.5 cm from Detector Pre- and Post-Cleaning Method for ZnO:In and ZnO:Ga 1.0%

reaction especially in the form of nitrate anions, the plausibility that those molecules are bonded to the surface and not being removed with minimal cleaning and drying following growth is high. Figure 4.17 displays the effects of quencher ions bonded to the surface of the substrate most likely in the form of nitrate ions or ammonia hydroxide molecules that were added to increase the population of hydroxide ions available to zinc ions to form ZnO as shown by Equations 2.14-2.21. Once the samples were thoroughly cleaned with both a water solvent in form of DI water and an alcohol solvent in the form of ethanol, the spectra were retaken with dramatically improved results as shown in Figure 4.17.

Following removal of quencher ions from the samples using the same cleaning method of DI water and ethanol as described in Section 3.3.2, alpha spectrums were taken over

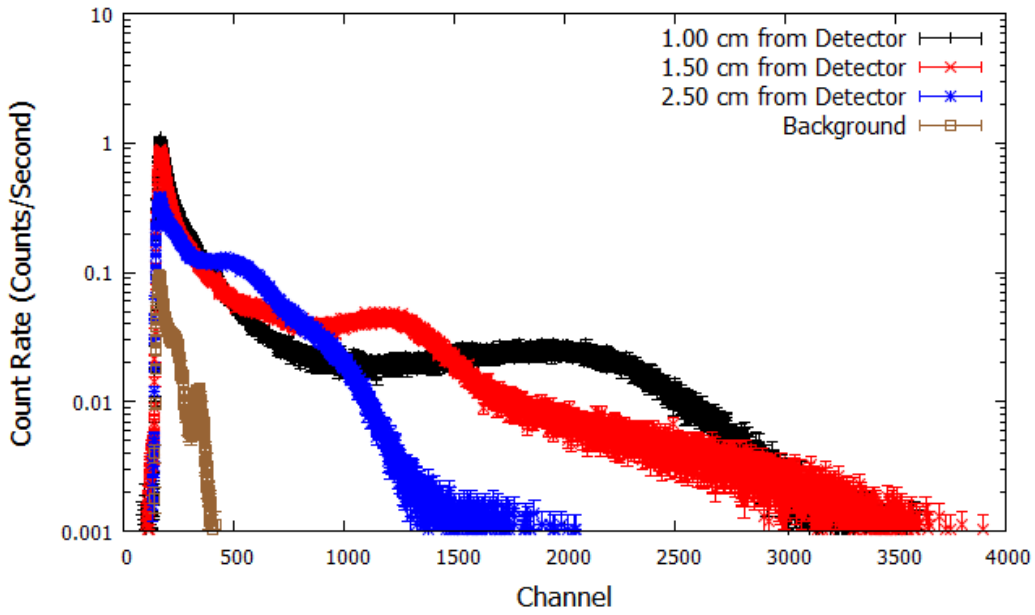

Figure 4.18: ^{241}Am Alpha Spectra with Undoped ZnO from 1.0 cm, 1.5 cm, and 2.5 cm

distances of 1.00 cm, 1.50 cm, and 2.50 cm for the undoped ZnO sample and at 2.5 cm for all doped samples. The reason for the taking all the remaining samples at 2.5 cm is that due to decreased lengths of nanorods in comparison to the undoped ZnO and the increased stopping power against lower energy heavy ions compared to that of the 5.54 MeV alpha emitted during alpha decay by Americium-241. The spectra for undoped ZnO over the various distances listed above is shown in Figure 4.18 and shows how the change in distance and energy of the alpha particles effect the spectra. As the distance was increased and the alpha particle energy decreased, the main detection peak shifted to the left as would be expected and intensity increased. The overall detection counts decreased which is also expected as the number of alpha particles making it through the collimator decreased. At the increased distance, the decreased angle of incidence needed to make it through the collimator resulted in a more monoenergetic source on the face of the detector.

To compare the effect of dopants on the detection of alpha particles, alpha spectra for each sample was taken at 2.5 cm resulting in average particle energy of 2.902 MeV as simulated in previous section using SRIM. Due to dopant, dopant concentration, and length

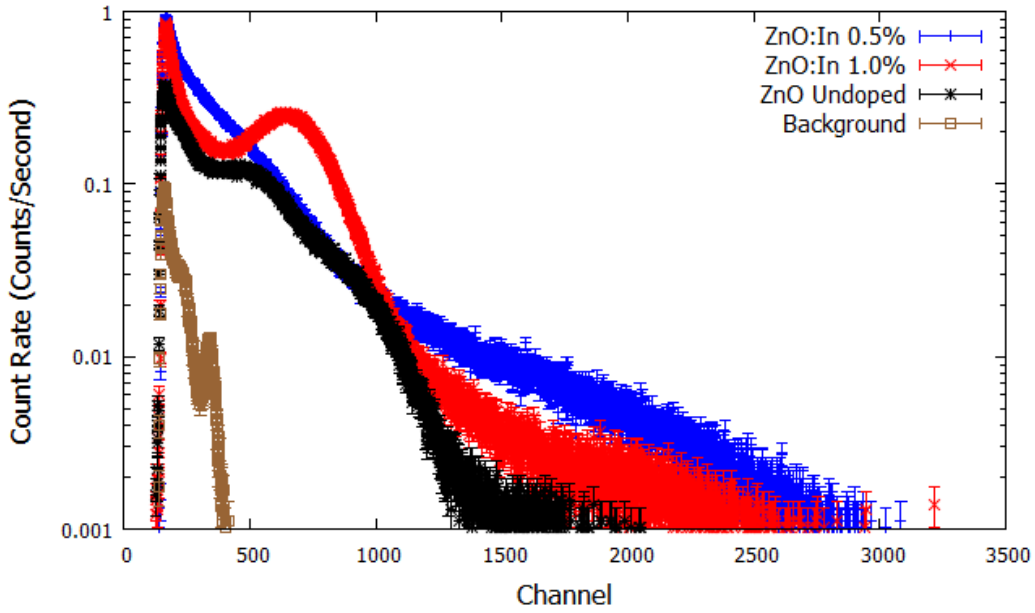

Figure 4.19: ^{241}Am Spectra at 2.5 cm from Detector for ZnO:In

Table 4.5: Peak information of undoped and doped ZnO at 2.5 cm

Sample	FWHM	Gross Counts	Peak Channel
Undoped ZnO	83.93	424487	540.40
ZnO:In 1.0%	262.55	1108599	662.23
ZnO:Ga 1.0%	1.41	342459	432.11
ZnO:Ga 0.5%	155.66	66504	822.84

of the nanorods differences, the alpha spectra will vary to a degree with respect to peak location and shape. The spectra for ZnO:In and ZnO:Ga for comparison of dopant concentration for each dopant and spectra for 1.0% and 0.5% for comparison of dopants at each concentration are shown in Figures 4.19/4.20 and 4.21/4.22, respectively. As has been shown in other research, the dopant does effect the peak location, response time, and photo-luminescence.[19] The main detection peak for ZnO:In 0.5% was not discernable from the rest of the spectra enough to gain peak information even though the appearance of a slight shoulder to the detection spectra. From the data listed in Table 4.5, it can be seen that the peak location when compared to average energy transfer from Table 4.4 does not follow the expected trend. This could be due to a number of reasons: higher quencher concentration in some, dopant mechanism for excitation decay time, or concentration ef-

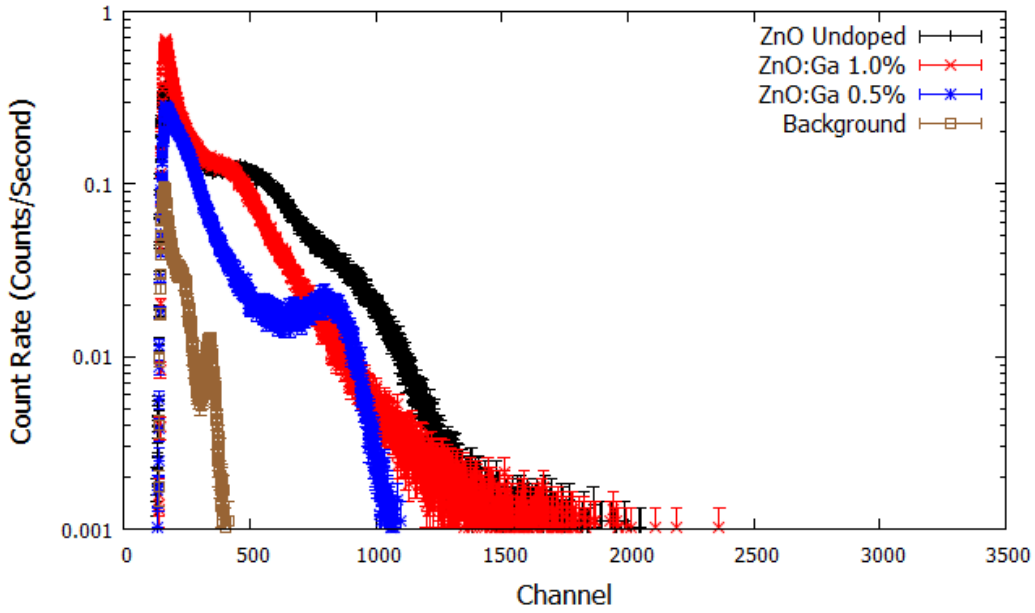

Figure 4.20: ^{241}Am Spectra at 2.5 cm from Detector for ZnO:Ga

fect on location of dopant (substitutional or interstitial). However, when comparing the dopant concentrations within each dopant the peaks do follow, but for confirmation would need two or three more sample concentrations to verify. In both the ZnO:In and ZnO:Ga, the sample with the simulated higher average energy concentration had a higher channel number for the center of the peak in comparison to the lower. As in [19], dopants even with the same energy alpha will have different peak location and peak shape.

Past small effects on decay time that dopants have and quantifiable effects like photoluminescence intensity, there is still a lot of research to be conducted into dopant and dopant concentrations in ZnO. The traditional use of activators in inorganic crystals does not have as strong an effect on ZnO due to its small band gap in comparison to other pure inorganic crystals. However, there has been research into bandgap engineering to both lower it and enlarge it.[63]

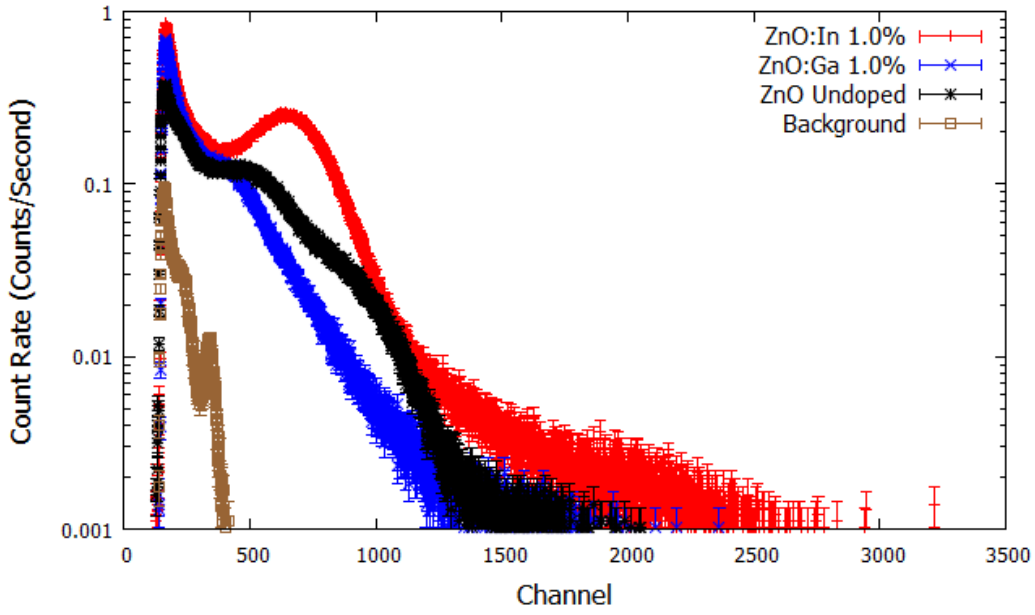

Figure 4.21: ^{241}Am Spectra at 2.5 cm from Detector comparison between dopants for 1.0% doped

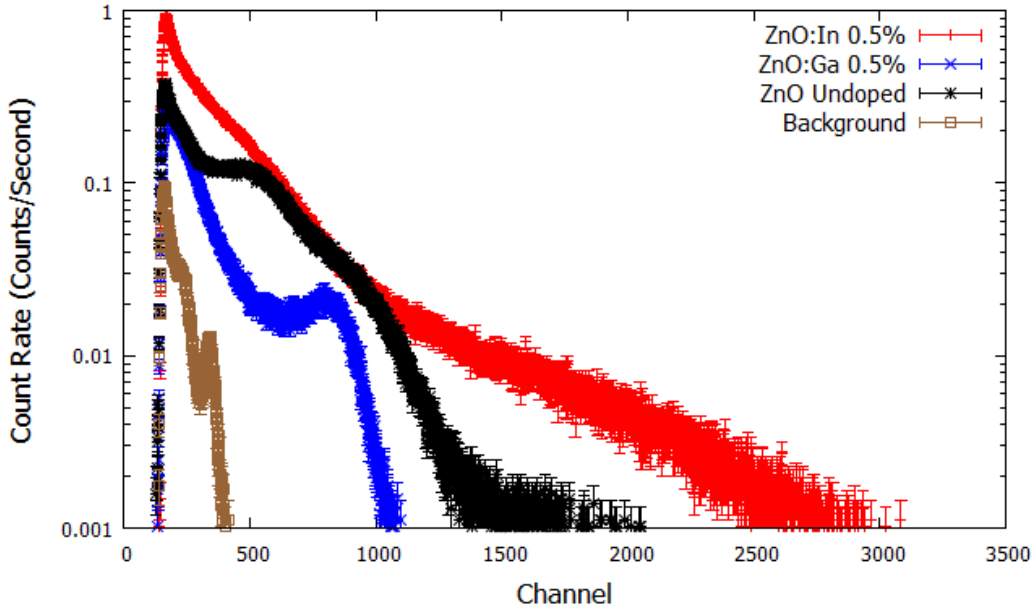

Figure 4.22: ^{241}Am Spectra at 2.5 cm from Detector comparison between dopants for 0.5% doped

CHAPTER 5
CONCLUSION

The goal of this project was to develop an alpha detector and procedure capable of being optimized for future research as a neutron detector. The scope of the project was broad in order to provide the best baseline possible for future research to build off of. There are however some conclusions that can be drawn from this work that will benefit the overall goal of the project in the future.

Fused silica while certain attributes are difficult to work with is a promising substrate for the other beneficial attributes. The surface energy of fused silica is low, but with further treatments can be enhanced and treated in a way that it will readily allow molecules to bond securely to the surface. The benefits of fused silica include cost which is lower than substrate such as single crystal quartz and transmission percentage for the near band edge emission of ZnO (380 nm) which is higher than that of quartz and ITO glass. The refractive index of fused silica is also closer to 1.5 than that of quartz resulting in less entrapped light, less internal reflection, and more light reaching the PMT.

Seeding of the substrate became a main focus due to the new substrate chosen for this project. Conventional dip coating methods proved to be ineffective at covering the surface in uniform seed layer capable of growing uniform uni-axial nanorods that promote the most efficient electron transport. Seed experiment one and subsequent growth on the seeded substrate did validate growth solution and an annealing procedure to be used in the future that will remove quenching molecules bonded to the surface more effectively then the cleaning method used. Spin coating is an effective means of seeding substrates with a uniform seed layer, but this method will need further research in order to bond the seed layer to the substrate to prevent separation of the nanorods from the substrate in annealing post-growth.

With respect to photo-luminescence and the optimization of the spectra to include reducing the broad emission without effecting the near band edge emission, there was some success. ZnO:In 0.5% presented the best photo-luminescence but had a poor scintillation spectra. This sample exhibited good suppression of the broad peak with minimal decrease in intensity of the near band edge emission. If the broad emission is in fact caused by zinc vacancies and the inclusion of dopants will reduce these vacancies, then with the exception of ZnO:In 1.0% the results followed as with each dopant the broad emission was reduced but the near band edge in gallium was also greatly affected. The reason for the effect on gallium is that interstitial placement of gallium ions in the lattice structure shifted the absorbance spectra to the right yielding a higher absorbance of the near band edge as discussed in Section 3.3.1.

Alpha detection was successful and yielded a definable peak for all samples except ZnO:In 0.5%, which could be attributed to quenching, dopant lattice location, or other factors. An additional goal of alpha detection was to determine the effects of varying alpha energy and the signal produced which was accomplished by attenuating the alpha particles with air and collimating out all but particles with small angle of incidence resulting in a near monoenergetic particle beam. This was achieved with some success as shown in the undoped ZnO spectra of the source at different distances. Quencher molecules played a significant role and without the additional thorough cleaning would have prevented detection of alpha particles.

CHAPTER 6

FUTURE WORK

6.1 Dopant

6.1.1 Cerium

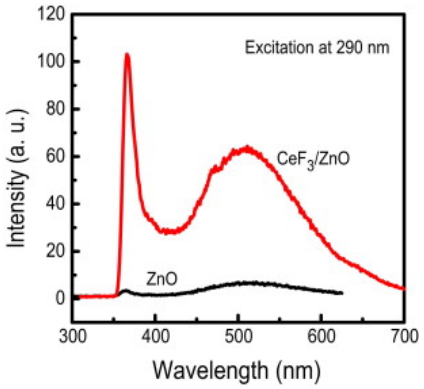

(a)

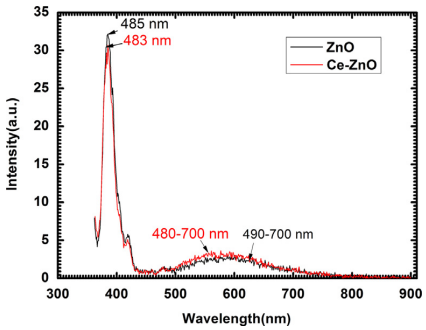

(b)

Figure 6.1: Photo-Luminescence spectra of (a) ZnO and ZnO/CeF_3 nanocomposite and (b) ZnO:Ce in solution [64]

Cerium has been used in a variety of ways in radiation detection from being used as an activator in crystal scintillators to being formed into an inorganic scintillator in the form of cerium bromide. In lanthanum bromide, a well-known fast inorganic scintillator with excellent energy discrimination, cerium is used as the activator. Cerium has been used in a limited fashion with respect to ZnO in the form of nanocomposite for alpha particle detection[64] and wet chemical synthesis of nanorods[65]. But, it has not been used as a dopant for an array of nanorods. Investigation into cerium doped nanorods for use as an alpha particle radiation detector and subsequent use with the incorporation of a ^{6}Li coating has not be undertaken. As can be seen in Figure 6.1, the intensity of the photo-luminescence spectra increases dramatically in the composite with the addition of CeF_3. The effect on nanorods as a dopant was insignificant; therefore, unless nanocomposites are researched

cerium does not show much promise in nanorod research.

6.1.2 Band Gap Engineering with Magnesium and Cadmium

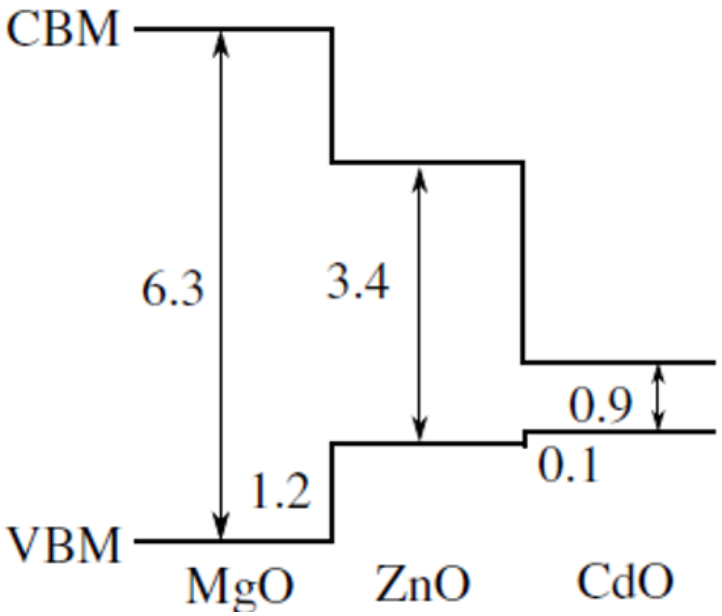

Figure 6.2: Band offsets at wurtzite MgO/ZnO and ZnO/CdO interfaces.[4, 63]

Doping ZnO nanorods with elements such as gallium, indium and aluminum is relatively easy as the inclusion of those elements will not affect the wurtzite structure of the nanorods. The inclusion of magnesium or cadmium effects the structure of the crystal significantly because the Mg-O and Cd-O bond forms a rock salt structure, but with modest amounts of dopant (less than 7.0%), the structure will retain its wurtzite structure [63]. The addition of magnesium and cadmium effectively engineers the bandgap and dependent on concentration can lead to band gaps ranging from 2.3 eV to 4.0 eV [63, 66, 67, 68, 69, 70, 71]. With band gap engineering using magnesium and cadmium, the band edge peak can be shifted.

6.2 Seeding

As the seeding technique was never perfected to yield a defined crystalline seed layer, there is future work to be done in spin coating. Dodecane-thiol procedure used in the first seed experiment could be utilized to assist in the bonding of the seed layer to the substrate. In addition to the dodecane-thiol, a higher pre-heating temperature and time of heating in between coatings may be required to achieve a better defined seed layer. A better defined crystalline seed layer that is bonded to the substrate should yield higher quality crystals that can undergo annealing treatments post growth that will better remove quenching molecules that effect scintillation.

Another method that has worked in the past with respect to this project is the use of sputtering to seed the substrate. If this method is available, then this would provide an alternate means, but the price and space required for such equipment far exceeds that of spin or dip coating. This method would also prevent doping of the seed layer which could benefit future research and the pre-development of substitution lattice positions for the dopant ion.

6.3 Nanorod Length

Of primary concern with respect to the nanorod length is its ability to fully absorb alpha particles incident on the detector to provide the best means for alpha spectroscopy. In the development of a neutron detector, it will be important to be able to absorb the alpha particle produced by the lithium or boron reaction with the thermal neutron. The length needed for detection of the lithium or boron reaction as calculated by [58] is 3.43 μm for the 1.47 MeV alpha of boron and 4.74 μm for the 2.05 MeV alpha of lithium, but the detection medium will need to be thicker due to straggling. For detection of the 5.54 MeV alpha of Am-241, the detector length/thickness will need to be over 15.59 μm. Use of polyethyleneimine (PEI) has be successfully used in research to lengthen the nanorods considerably. [72, 73,

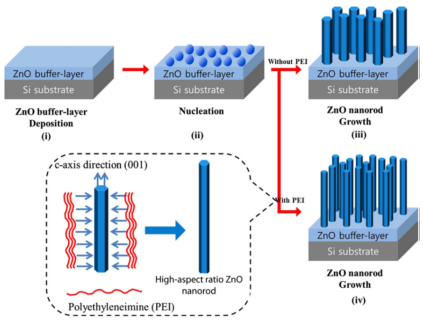

(a) Schematic for growth mechanism of ZnO with/without PEI[72]

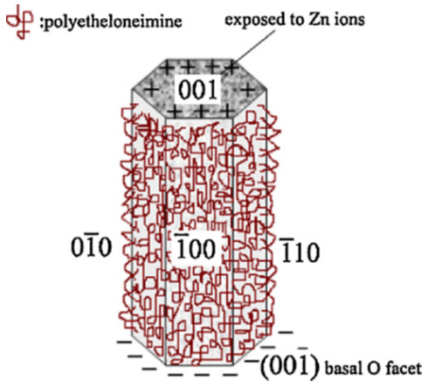

(b) PEI mechanism on ZnO nanorod [74]

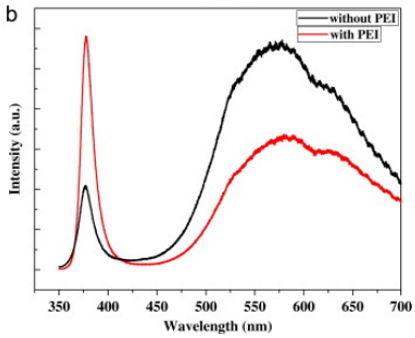

(c) Photo-luminescence spectra with and without PEI

Figure 6.3: Mechanism of PEI effects on vertical growth along c-axis on ZnO nanorods as shown in (a) [72] and (b) [74]. Effects of PEI on photo-luminescence spectra are shown in (c) by [72]

74]

The PEI mechanism for lengthening the nanorods is through constricting the lateral growth resulting in preferential growth along the c-axis as shown in Figure 6.3. By restricting the growth laterally and enhancing the growth vertically, the length of the nanorod is significantly enhanced while the diameter is smaller. What has not be tested is the effect of decreasing the diameter has on its radiation hardness and durability as a detector when exposed to high radiation fields over long periods of time. The effects of PEI on the photo-luminescence spectra is promising as shown in 6.3c, but the reason for the enhancement of the near band edge and suppression of the broad green emission is unclear. It could be attributed to the decrease in impurities within lattice yielding a higher quality ZnO phase of growth.[72]

6.4 Lithium or Boron Coating

Before the type of neutron absorber and its effects are discussed, an understanding of neutron interactions with matter is needed. In general, there are two types of interactions that a neutron will have with matter, direct interaction and compound-nucleus reaction. Direct interaction deals with interactions that do not involve the core of the nucleus that the neutron is interacting with. The main type of direct interaction is known as potential scattering in that the neutron is scattered away from the nucleus due to the presence of the strong nuclear force within the nucleus and is also known as "shape scattering" and generally takes less than 10^{-22} s.[7] Compound-nucleus reactions are far more complicated due to the different types of reactions and particle physics that must be taken into account that depend on neutron energy, binding energy of nucleons, angular and orbital momentum, and many other factors. These reactions have a range of reaction time 10^{-18} s to 10^{-14} s with the main reaction after being the release of the excess energy via gamma photon emission.[7]

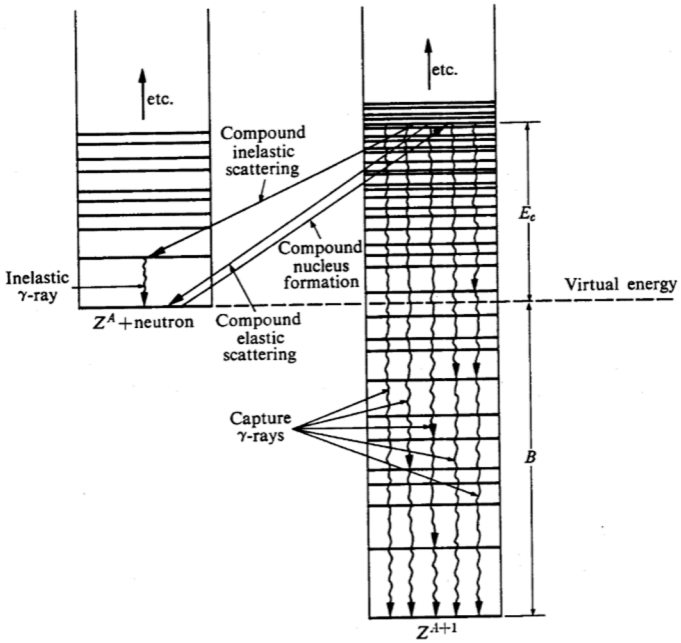

Figure 6.4: Diagram showing role of compound nucleus in neutron interactions.[75]

Compound nucleus reactions that occur once a neutron is absorbed depend on many

factors and can take many paths which generally depend on Q-value, binding energy per nucleon, time reaction takes, and different advanced particle physics subjects.

$$B(orQ) = \Delta Mc^2 \tag{6.1}$$

$$E_c = (\frac{A}{A+1})E_n \tag{6.2}$$

$$E_c' = (\frac{A}{A+1})E_n + [m_n + M(^AX) - M(^{A+1}X)]c^2 \tag{6.3}$$

Using Equation 6.1 and referencing B or Q from Figure 6.4, the energy level that the compound nucleus is at if the neutron enters the nucleus with zero energy can be determined.[7] The energy level of the nucleus if the neutron enters the nucleus with is the E_c value from Equation 6.2 added to the B or Q value from Equation 6.1 and is generally known as E_c' and shown in Equation 6.3. These values play a large role into the different types of reactions that can occur because a reaction can only take place if there is an energy level available for that particular reaction. Some of the reactions that can occur following absorption of the neutron are [n,α], [n,p], [n,2n], and [n,γ] to name a few. Each of these reactions have what is called a cross section which is defined a probability for the reaction to occur and normally expressed in a units of *barns* which is 10^{-24} cm^2 and denoted by the symbol σ.[76]

The non-elastic cross sections for different reactions such as [n,γ], [n,α], and [n,p] follow what is known as a "$\frac{1}{v}$" law when dealing with energies lower than that of the resonance region and can be seen in 6.5. The "$\frac{1}{v}$" relationship shows the difficulty of neutron detection and material identification because as the energy of the neutron increases and in some cases 10+ MeV the cross section for a non-elastic reaction is very small. This relationship can be seen in Figure 6.5 for some of the key reactions used in the detection of neutrons.

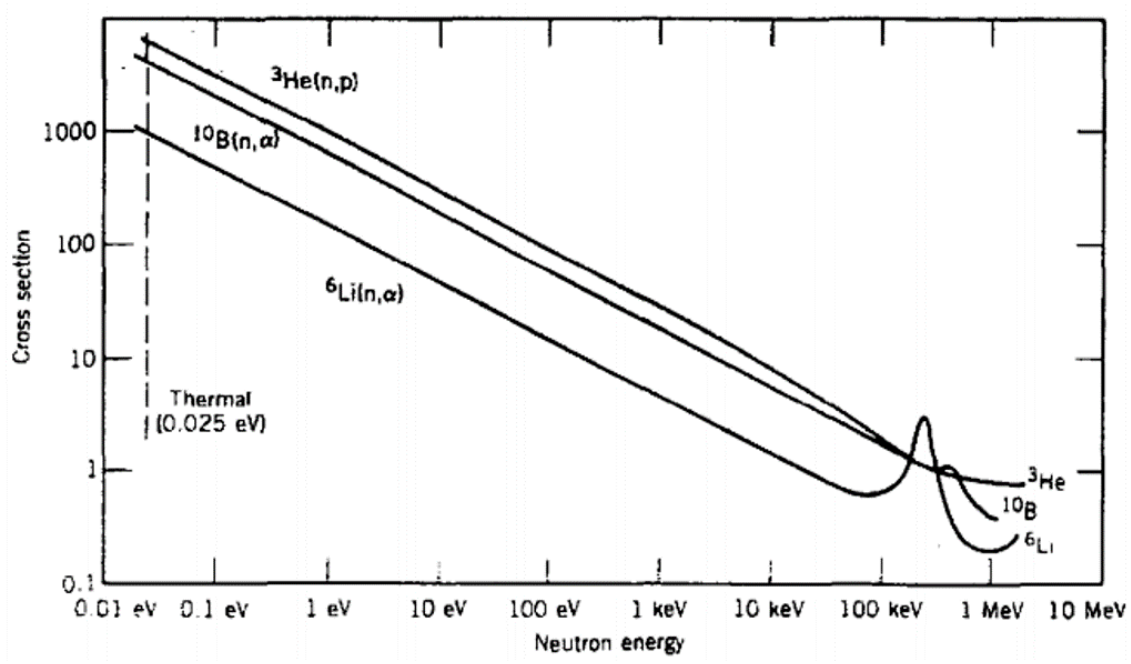

Figure 6.5: Neutron cross sections for ^{3}He[n,p], ^{6}Li[n,α], and ^{10}B[n,α] The cross section shows the 1/v behavior for E¡1 keV, but begins to show resonances above 100keV.[77]

6.4.1 Key Reactions for Neutron Detection

There are the two neutron interaction reactions with matter that of use in neutron detection research for ZnO, ^{10}B and ^{6}Li. These interactions are chosen largely for their large cross sections as shown in Figure 6.5. These reactions are also chosen for their large Q value which means that the kinetic energy of the reaction products is determined solely by the Q value and the energy of the incoming neutron is negligible.[9] Only the reaction of boron and lithium will be discussed in this chapter for future research into ZnO as a neutron detector.

$$E_x + E_y = Q \tag{6.4}$$

$$\sqrt{2m_x E_x} = \sqrt{2m_y E_y} \tag{6.5}$$

The energy of the products can be determined by Equations 6.4 and 6.5 and will be used in the following paragraphs to show the energy of the products. The symbols x and y denote

the element and the particle (α,^{3}H, etc).

$$^6_3Li +^1_0 n \rightarrow^3_1 H + \alpha \tag{6.6}$$

For lithium coating Equation 6.6 shows the reaction of interest for neutron detection. The energy values $E_{^3H}$ and E_α are 2.73 MeV and 2.05 MeV respectively for a reaction with a thermal neutron where the energy contributed by the initial neutron is negligible.[9] The reaction products are released 180^o from each other; therefore, their uses in a neutron converter will be limited to only events that yield alpha particles in the direction of the detector which will decrease efficiency.

$$^{10}_5B +^1_0 n \rightarrow^7_3 Li + \alpha \tag{6.7}$$

For a boron coating, Equation 6.7 depicts the reaction that a neutron has with ^{10}B. The energy values for the reaction products are 0.84 MeV and 1.47 MeV for E_{Li} and E_α respectively.[9] The draw for boron for this detector is there is a higher cross section and the energy of the alpha particle would require a shorter nanorod then lithium.

6.4.2 Coating ability

If well grown nanorods are securely bonded to the surface of the substrate and can be annealed at high temperatures, the preferred method would be to use a vacuum evaporator to deposit a thin film of boron-10 or lithium-6 onto the surface of the nanorods that have been grown to slightly past the range of their respective alpha particles in the detector volume. With a thin film of boron or lithium deposited, the overall view of detector cross section would be similar to that of case A or B of Figure 6.6. As discussed above, the detection efficiency of the detector would be quite low but methods to improve would be to grow an additional layer of ZnO on top of the converter layer, but the ability of light from the top detection volume to reach the PMT would need to be analyzed. Other

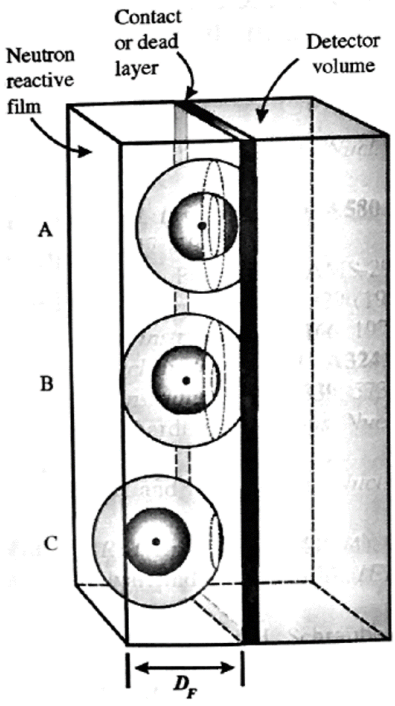

Figure 6.6: Sketch of converter layer of thickness D_F in contact with detector[9, 78]

methods would be to use a solution to deposit a mixture containing a solvent with lithium-6 molecules and use thermal decomposition to secure the lithium/boron to the surface of the crystals.

Appendices

APPENDIX A

EXPERIMENTAL EQUIPMENT

A.1 Growth Equipment

A.1.1 Chemicals

The following chemicals were used in substrate preparation, seeding, and growth processes. All chemicals were purchased through Sigma Aldrich at highest purity available.

Table A.1: Chemical Seeding Information [79][80]

Chemical Name	Formula	M.W. ($\frac{g}{mol}$)	Density ($\frac{g}{mL}$)	Purity
2-Methoxyethanol	$CH_3OCH_2-CH_2OH$	76.09	0.965	99.8%
Ethanol	CH_3CH_2OH	46.07	0.789	99.5%
Ethanolamine (MEA)	$NH_2CH_2-CH_2OH$	61.08	1.012	99.0%
Zinc Acetate Dihydrate	$Zn(CH_3COO)_2\cdot 2H_2O$	219.51	N/A	98.0%
Acetone	CH_3COCH_3	58.08	0.7845	99.5%
Isopropanol	$(CH_3)_2CHOH$	60.10	0.7851	99.7%

Table A.2: Chemical Growth Information [79]

Chemical Name	Formula	M.W. ($\frac{g}{mol}$)	Density ($\frac{g}{mL}$)	Purity
Ammonia Hydroxide Solution	N/A	N/A	N/A	28-30%
Zinc Nitrate hexahydrate	$Zn(NO_3)_2 \cdot 6H_2O$	297.49	N/A	98.0%
Gallium(III) nitrate hydrate	$Ga(NO_3)_3 \cdot xH_2O$	255.74	N/A	99.9%
Sodium Citrate dihydrate	$HOC(COONa)(CH_2COONa)_2 \cdot 2H_2O$	294.10	N/A	99.0%
Indium (III) nitrate hydrate	$In(NO_3)_3 \cdot xH_2O$	300.83	N/A	99.9%
Hexamethylene-tetramine (HMTA)	$C_6H_{12}N_4$	140.19	N/A	99%
10% H_2 balance N_2				

A.1.2 Seeding

Seeding experiment 1 was conducted in TLD Laboratory in Boggs, and seeding experiment 2 was conducted in the North Avenue Research Area (NARA) in the Carbon Neutral Energy Systems (CNES) Lab courtesy of Dr Shannon Yee.

Table A.3: Equipment Needed for Seed Experiment 1

Hardware	***Chemicals***
$100 - 1000\mu L$ Pipette	Ethanol
disposable pipette tips	Dodecane Thiol
applicator brush	Isopropanol
furnace	ZnO nanoparticles
graduated cylinder (100mL)	DI Water
scoopla	
substrate (fused silica)	
support stand	
magnetic stirrer	
weight paper	
scale	
container for solution	

Table A.4: Equipment Needed for Seed Experiment 2

Hardware	***Chemicals***
$100 - 1000\mu L$ Pipette	Methoxyethanol
disposable pipette tips	Zinc Acetate
applicator brush	Isopropanol
furnace	Acetone
scoopla	Monoethanolamine(MEA)
substrate (fused silica)	
magnetic stirrer	
weight paper	
scale	
container for solution	
Spin Coater	
Oven	

Figure A.1: VTC-100 Programmable Spin Coater

Figure A.2: VWR Forced Air Oven Model 410

Figure A.3: SharperTek TOV120-3L Heated Ultrasonic Cleaner

Figure A.4: Lindberg Blue M Furnace

A.1.3 Growth

The following equipment was used in the growth of ZnO nanorods and was conducted in TLD Laboratory in Boggs.

Table A.5: Equipment Needed for Growth

Hardware	***Chemicals***
$100 - 1000\mu L$ Pipette	Sodium Citrate
disposable pipette tips	Zinc Nitrate Hexahydrate
weigh boats	hexamethylene (HTMA)
scale	dopant (Gallium, Indium, etc)
graduated cylinder (100mL)	DI Water
scoopla	Ammonia Hydroxide
seeded substrate	H_2 balance Nitrogen
glassware as needed	
teflon tap	
pH meter	

Figure A.5: Yamato DKN400 Mechanical Convection Oven

A.2 Characterization Equipment

A.2.1 Material and Structural Analysis Equipment

Scanning electron microscope imaging was conducted at the Paper Tricentennial Building with training conducted courtesy of Yolande Berta.

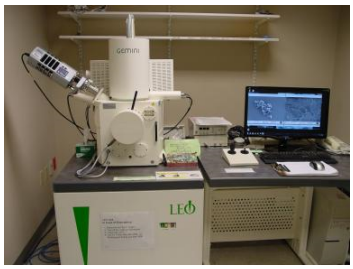

Figure A.6: LEO1530 Scanning Electron Microscope with Energy Dispersive Spectroscopy

A.2.2 Photo-luminescence Spectra Equipment

Photo-luminescence spectra were taken in Dr Hertel's Radiation Detection Laboratory.

Figure A.7: Kimmon He-Cd Dual Wavelength Laser

A.3 Radiation Detection Equipment

Radiation detection spectra were taken in Dr Hertel's Radiation Detection Laboratory.

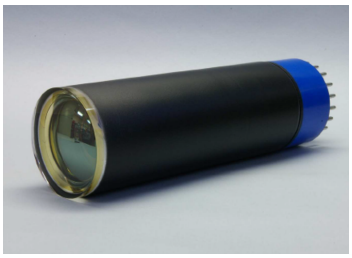

Figure A.8: Philips XP2020 Photomultiplier Tube

Figure A.9: Ortec Model 113 Scintillation Preamplifier

(a) Ortec Model 572 Shaping Amplifier

(b) Ortec Model 926 ADCAM MCB

(c) Canberra Model 3002D High Voltage

Figure A.10: NIM Bin Equipment

REFERENCES

[1] NobelPrize.org. (Dec. 15, 2016). Wilhelm conrad rntgen - facts. N. M. A. 2014, Ed.

[2] J. S.N.J.T.M.D.K. C. Cooper, "Update on a zno:ga alpha particle detector for a portable neutron generator for the nuclear materials identification system (nmis)," Oak Ridge National Laboratory, Purdue University Physics Department and Applied Physics Laboratory.

[3] J. C. Cooper, D. S. Koltick, and et. al, "Evaluation of zno(ga) coatings as alpha particle transducers within a neutron generator," Nucl Instrum Methods Phys Res , Sect A, 505, no., pp. 498–501, 2003.

[4] A. Janotti and C. G. V. de Walle, "Absolute deformation potentials and band alignment of wurtzite ZnO, MgO, and CdO," Phys. Rev. B, 75, no., 2007.

[5] F. Tuomisto, K. Saarinen, D. C. Look, and G. C. Farlow, "Introduction and recovery of point defects in electron-irradiated zno," Phys. Rev. B, 72, no., 2005.

[6] D. C. Look, J. W. Hemsky, and J. R. Sizelove, "Residual native shallow donor in zno," Phys. Rev. Lett., 82, no., pp. 2552–2555, 1999.

[7] C. K. Wang, Atoms, Nuclei & Interactions of Ionizing Radiation with Matter. Congnella Academic Publishing, 2017, ISBN: 9781516501731.

[8] J. Birks, The Theory and Practice of Scintillation Counting. Elsevier BV, 1964.

[9] G. Knoll, Radiation Detection and Measurement. Wiley-Blackwell, 2014.

[10] J. R. Lakowicz and G. Weber, "Quenching of fluorescence by oxygen. probe for structural fluctuations in macromolecules," Biochemistry, 12, no., pp. 4161–4170, 1973.

[11] A. P. Darmanyan and W. S. Jenks, "[22] synthetic singlet oxygen quenchers," no., pp. 226–241, 2000.

[12] M. Arık, N. Çelebi, and Y. Onganer, "Fluorescence quenching of fluorescein with molecular oxygen in solution," J. Photochem. Photobiol., A, 170, no., pp. 105–111, 2005.

[13] M. Polyanskiy. (Mar. 13, 2017). Refractive index.

[14] W. L. Bond, "Measurement of the refractive indices of several crystals," J. Appl. Phys., 36, no., pp. 1674–1677, 1965.

[15] I. H. Malitson, "Interspecimen comparison of the refractive index of fused silica," J. Opt. Soc. Am., 55, no., p. 1205, 1965.

[16] C. Tan, "Determination of refractive index of silica glass for infrared wavelengths by ir spectroscopy," J. Non-Cryst. Solids, 223, no., pp. 158–163, 1998.

[17] M. R. Querry, "Optical constants," Contractor Report, no., 1985.

[18] Handbook of Optics, 3rd. McGraw-Hill, 2009, vol. 4.

[19] J. S. Neal, N. C. Giles, X. Yang, R. A. Wall, K. B. Ucer, R. T. Williams, D. J. Wisniewski, L. A. Boatner, V. Rengarajan, J. Nause, and B. Nemeth, "Evaluation of melt-grown, zno single crystals for use as alpha-particle detectors," IEEE, 55, no., pp. 1397–1403, 2008.

[20] G Perillat-Merceroz, P. H. Jouneau, G Feuillet, R Thierry, M Rosina, and P Ferret, "Mocvd growth mechanisms of zno nanorods," J. Phys. Conf. Ser., 209, no., p. 012 034, 2010.

[21] S. Blackwell, R. Smith, S. D. Kenny, J. M. Walls, and C. F. Sanz-Navarro, "Modelling the growth of zno thin films by pvd methods and the effects of post annealing," J. Phys.: Condens. Matter, 25, no., p. 135 002, 2013.

[22] N. Lehraki, M. Aida, and et. al, "Zno thin films deposition by spray pyrolysis: Influence of precursor solution properties," Curr. Appl Phys., 12, no., pp. 1283–1287, 2012.

[23] T. Yoshida, D. Komatsu, and et. al, "Mechanism of cathodic electrodeposition of zinc oxide thin films from aqueous zinc nitrate baths," Thin Solid Films, 451-452, no., pp. 166–169, 2004.

[24] G. N. Soaram Kim, "Effects of doping with al, ga, and in on structural and optical properties of zno nanorods grown by hydrothermal method," Bull. Korean Chem. Soc., 34, no., pp. 1205–1211, 2013.

[25] M. A. Mahmood, S. Jan, I. A. Shah, and I. Khan, "Growth parameters for films of hydrothermally synthesized one-dimensional nanocrystals of zinc oxide," Int J Photoenergy, 2016, no., pp. 1–12, 2016.

[26] S. Xu, C. Lao, B. Weintraub, and Z. L. Wang, "Density-controlled growth of aligned ZnO nanowire arrays by seedless chemical approach on smooth surfaces," J. Mater. Res., 23, no., pp. 2072–2077, 2008.

[27] H. Morkoc and m. zgr, Zinc Oxide. Wiley VCH Verlag GmbH, Jan. 14, 2009, ISBN: 978-3-527-40813-9.

[28] R. Jayakrishnan, "Aluminum doped ZnO thin films using chemical spray pyrolysis," OALib, 02, no., pp. 1–10, 2015.

[29] Phosphor Handbook. CRC PR INC, Dec. 11, 2006, 1051 pp., ISBN: 9780849335648.

[30] A. B. Djurišić, Y. H. Leung, K. H. Tam, Y. F. Hsu, L Ding, W. K. Ge, Y. C. Zhong, K. S. Wong, W. K. Chan, H. L. Tam, K. W. Cheah, W. M. Kwok, and D. L. Phillips, "Defect emissions in ZnO nanostructures," Nanotechnology, 18, no., p. 095 702, 2007.

[31] S. S. Shinde, P. S. Shinde, C. H. Bhosale, and K. Y. Rajpure, "Optoelectronic properties of sprayed transparent and conducting indium doped zinc oxide thin films," J. Phys. D: Appl. Phys., 41, no., p. 105 109, 2008.

[32] E. Burstein, "Anomalous optical absorption limit in InSb," Phys. Rev., 93, no., pp. 632–633, 1954.

[33] H.-C. Wu, Y.-C. Peng, and C.-C. Chen, "Effects of ga concentration on electronic and optical properties of ga-doped zno from first principles calculations," Opt. Mater., 35, no., pp. 509–515, 2013.

[34] Y.-S. Lee, Y.-C. Peng, J.-H. Lu, Y.-R. Zhu, and H.-C. Wu, "Electronic and optical properties of ga-doped zno," Thin Solid Films, 570, no., pp. 464–470, 2014.

[35] Y.-S. Choi, D.-K. Hwang, M.-S. Oh, K.-P. Hong, V. T. Em, H.-W. Choi, and S.-J. Park, "Growth and characterization of gallium-doped zno films for -particle scintillators," J Electrochem Soc, 155, no., H909, 2008.

[36] X. Wang, Y. Tao, H. Zhao, M. Fu, D. He, and Y. Wang, "Growth and physical properties of zno rod arrays that integrally match the geometries of photoresists with hole sizes larger than rods habit diameters," Journal of Alloys and Compounds, 704, no., pp. 131–140, 2017.

[37] J. Yang, J. Wang, X. Li, J. Lang, F. Liu, L. Yang, H. Zhai, M. Gao, and X. Zhao, "Effect of polar and non-polar surfaces of zno nanostructures on photocatalytic properties," Journal of Alloys and Compounds, 528, no., pp. 28–33, 2012.

[38] L. Jia, W. Cai, H. Wang, and H. Zeng, "Polar-field-induced double-layer nanostructured zno and its strong violet photoluminescence," Crystal Growth & Design, 8, no., pp. 4367–4371, 2008.

[39] P. Hausladen and et. al, "An alpha particle detector for a portable neutron generator for the nuclear materials identification system (NMIS)," Nucl. Instrum. Methods Phys. Res., Sect. B 241, no., pp. 835–838, 2005.

[40] Q. Peng and Y. Qi, "ZnO nanowires and their application for solar cells," no., 2011.

[41] C Coskun, D. C. Look, G. C. Farlow, and J. R. Sizelove, "Radiation hardness of ZnO at low temperatures," Semiconductor Science and Technology, 19, no., pp. 752–754, 2004.

[42] A Burlacu, V. V. Ursaki, V. A. Skuratov, D Lincot, T Pauporte, H Elbelghiti, E. V. Rusu, and I. M. Tiginyanu, "The impact of morphology upon the radiation hardness of ZnO layers," Nanotechnology, 19, no., p. 215 714, 2008.

[43] D. C. Look, D. C. Reynolds, J. W. Hemsky, R. L. Jones, and J. R. Sizelove, "Production and annealing of electron irradiation damage in ZnO," Applied Physics Letters, 75, no., pp. 811–813, 1999.

[44] K. Saarinen, T. Suski, I. Grzegory, and D. C. Look, "Thermal stability of isolated and complexed ga vacancies in GaN bulk crystals," Phys. Rev. B, 64, no., 2001.

[45] O. Ltd. (2016). Spin coating: A guide to theory and techniques.

[46] D. C. Company, Ethanolamines, 2003.

[47] F. D. S. Corps. (2006). Surface tension values of some common test liquids for surface energy analysis.

[48] NCBI. (Nov. 12, 2016). 2-methoxyethanol.

[49] G. A. Parks, "Surface and interfacial free energies of quartz," J. Geophys. Res., 89, no., pp. 3997–4008, 1984.

[50] J. S. Kim, R. H. Friend, and F. Cacialli, "Surface energy and polarity of treated indiumtinoxide anodes for polymer lightemitting diodes studied by contact-angle measurements," J. Appl. Phys., 86, no., p. 2774, 1999.

[51] M. S. Farhan, E. Zalnezhad, A. R. Bushroa, and A. A. D. Sarhan, "Electrical and optical properties of indium-tin oxide (ito) films by ion-assisted deposition (iad) at room temperature," International Journal of Precision Engineering and Manufacturing, 14, no., pp. 1465–1469, 2013.

[52] U. Wafer. (). Fused silica, ito glass, and single crystal quartz.

[53] I. Gonzalez-Valls and M. Lira-Cantu, "Vertically-aligned nanostructures of ZnO for excitonic solar cells: A review," Energy Environ Sci, 2, no., pp. 19–34, 2009.

[54] S. Baruah, C. Thanachayanont, and J. Dutta, "Growth of zno nanowires on non-woven polyethylene fibers," Science and Technology of Advanced Materials, 9, no., p. 025 009, 2008.

[55] E. M. Claesson and A. P. Philipse, "Thiol-functionalized silica colloids, grains, and membranes for irreversible adsorption of metal(oxide) nanoparticles," Colloids Surf., A, 297, no., pp. 46–54, 2007.

[56] L. Znaidi, "Solgel-deposited zno thin films: A review," Materials Science and Engineering, 174, no., pp. 18–30, 2010.

[57] L. Znaidi, G. S. Illia, S. Benyahia, C. Sanchez, and A. Kanaev, "Oriented zno thin films synthesis by solgel process for laser application," Thin Solid Films, 428, no., pp. 257–262, 2003.

[58] J. Biersack and J. Ziegler, Results achieved using srim, 1984,1989,1992,1998,2008.

[59] Radiological health handbook. Office of Scientific and Technical Information (OSTI), 1970.

[60] G.-C. Yi, C. Wang, and W. I. Park, "ZnO nanorods: Synthesis, characterization and applications," Semiconductor Science and Technology, 20, no., S22–S34, 2005.

[61] I. Kretzschmar, R. Chang, and K. Ithisuphalap, "Impact of particle shape on electron transport and lifetime in zinc oxide nanorod-based dye-sensitized solar cells," AIMS Materials Science, 3, no., pp. 51–65, 2016.

[62] J. H. Lim, S. M. Lee, H.-S. Kim, H. Y. Kim, J. Park, S.-B. Jung, G. C. Park, J. Kim, and J. Joo, "Synergistic effect of indium and gallium co-doping on growth behavior and physical properties of hydrothermally grown ZnO nanorods," Scientific Reports, 7, no., p. 41 992, 2017.

[63] A. Janotti, "Fundamentals of zinc oxide as a semiconductor," Rep. Prog. Phys., 72, no., p. 126 501, 2009.

[64] S. Sahi and W. Chen, "Luminescence enhancement in CeF3/ZnO nanocomposites for radiation detection," Radiat. Meas., 59, no., pp. 139–143, 2013.

[65] N. Sinha, G. Ray, S. Bhandari, S. Godara, and B. Kumar, "Synthesis and enhanced properties of cerium doped zno nanorods," Ceram. Int., 40, no., pp. 12 337–12 342, 2014.

[66] A. Ohtomo, M. Kawasaki, T. Koida, K. Masubuchi, H. Koinuma, Y. Sakurai, Y. Yoshida, T. Yasuda, and Y. Segawa, "Mgxzn1-xo as a ii-vi widegap semiconductor alloy," Applied Physics Letters, 72, no., pp. 2466–2468, 1998.

[67] A. Ohtomo, K. Tamura, M. Kawasaki, T. Makino, Y. Segawa, Z. K. Tang, G. K. L. Wong, Y. Matsumoto, and H. Koinuma, "Room-temperature stimulated emission of excitons in zno mg,zno superlattices," Applied Physics Letters, 77, no., pp. 2204–2206, 2000.

[68] Y. Jin, B. Zhang, S. Yang, Y. Wang, J. Chen, H. Zhang, C. Huang, C. Cao, H. Cao, and R. Chang, "Room temperature uv emission of mgxzn1-xo films," Solid State Commun., 119, no., pp. 409–413, 2001.

[69] T. Gruber, C. Kirchner, R. Kling, F. Reuss, A. Waag, F. Bertram, D. Forster, J. Christen, and M. Schreck, "Optical and structural analysis of zncdo layers grown by metalorganic vapor-phase epitaxy," Applied Physics Letters, 83, no., pp. 3290–3292, 2003.

[70] T. Gruber, C. Kirchner, R. Kling, F. Reuss, and A. Waag, "Znmgo epilayers and zno - znmgo quantum wells for optoelectronic applications in the blue and uv spectral region," Applied Physics Letters, 84, no., pp. 5359–5361, 2004.

[71] T. Makino, Y. Segawa, M. Kawasaki, A. Ohtomo, R. Shiroki, K. Tamura, T. Yasuda, and H. Koinuma, "Band gap engineering based on mgxzn1-xo and cdyzn1-yo ternary alloy films," Applied Physics Letters, 78, no., pp. 1237–1239, 2001.

[72] H.-S. Choi, M. Vaseem, and et. al, "Growth of high aspect ratio ZnO nanorods by solution process: Effect of polyethyleneimine," J. Solid State Chem., 189, no., pp. 25–31, 2012.

[73] Q. Huang, L. Fang, X. Chen, and M. Saleem, "Effect of polyethyleneimine on the growth of ZnO nanorod arrays and their application in dye-sensitized solar cells," Journal of Alloys and Compounds, 509, no., pp. 9456–9459, 2011.

[74] Y. Zhou, W. Wu, G. Hu, H. Wu, and S. Cui, "Hydrothermal synthesis of zno nanorod arrays with the addition of polyethyleneimine," Mater. Res. Bull., 43, no., pp. 2113–2118, 2008.

[75] Lamarsh, Introduction to Nuclear Reactor Theory, 3. AIP Publishing, 1967, vol. 20, pp. 110–111.

[76] J. R. Lamarsh and A. J. Baratta, Introduction to Nuclear Engineering, 3rd ed. 2001, ISBN: 978-0201824988.

[77] K. S. Krane, Introductory Nuclear Physics, 1. AIP Publishing, 1989, vol. 42, pp. 78–78.

[78] D. McGregor, M. Hammig, and et. al, "Design considerations for thin film coated semiconductor thermal neutron detectors i: Basics regarding alpha particle emitting neutron reactive films," Nucl. Instrum. Methods Phys. Res., Sect. A, 500, no., pp. 272–308, 2003.

[79] Sigma-Aldrich. (Jan. 17, 2017). Various chemicals as listed.

[80] S. I. Services, Ed., Acetone, Isopropanol, Mar. 30, 2017.